

Efficient Two-Qubit Pulse Sequences Beyond CNOT

D. Zeuch¹ and N.E. Bonesteel²

¹ Peter Grünberg Institut: Theoretical Nanoelectronics, Research Center Jülich, Germany

² Department of Physics and National High Magnetic Field Laboratory, Florida State University, Tallahassee, FL 32310, USA

(Dated: December 21, 2024)

We design efficient two-qubit controlled-rotation gates with arbitrary angle for exchange-only spin-based quantum computation carried out by sequences of exchange pulses acting on encoded three-spin qubits. Two constructions are given. The first is motivated by an analytic derivation of the efficient Fong-Wandzura sequence for an exact CNOT gate. This analytic derivation, briefly reviewed here, is based on a type of elevation of a simple five-pulse sequence consisting only of SWAP or trivial pulses, which captures the essential structure of the Fong-Wandzura sequence. To obtain two-qubit sequences beyond CNOT, we start with a modified five-pulse sequence consisting of four SWAP pulses and one pulse of arbitrary duration. We then show this sequence can be elevated, in a fashion similar to that used in the analytic derivation of the Fong-Wandzura sequence, to yield a two-qubit sequence that carries out a controlled-rotation gate with arbitrary angle. The second construction streamlines a class of arbitrary CPHASE pulse sequences found earlier by analytically designing sequences acting first on only three, then four, and finally five spins. Both constructions are based on building two-qubit sequences out of subsequences with special properties that render each step of the construction analytically tractable.

I. INTRODUCTION

In their original proposal for spin-based quantum computation, Loss and DiVincenzo envisioned a quantum computer in which every qubit is encoded into the two-dimensional Hilbert space of a spin- $\frac{1}{2}$ particle, such as the spin of an electron trapped in a quantum dot [1]. Universal quantum gates can be carried out by adiabatically pulsing the Heisenberg exchange Hamiltonian $\mathbf{J}\mathbf{S}_i \cdot \mathbf{S}_j$ between pairs of spins, if combined with controlling time-dependent magnetic fields that are local in the spin positions. In a subsequent proposal, in which qubits are represented by pairs of spin- $\frac{1}{2}$ particles, universality is achieved through control of the Heisenberg exchange Hamiltonian supplemented by a static magnetic field gradient within each two-spin qubit [2]. If, however, logical qubits are encoded using at least three spin- $\frac{1}{2}$ particles, controlled exchange by itself is a universal resource for quantum computation [3, 4].

A comprehensive review of computing schemes based on various three-spin qubit implementations is given in Ref. [5]. In the present work we focus on the exchange-only proposal introduced in Ref. [6], in which each qubit is encoded using three spin- $\frac{1}{2}$ particles, and quantum gates are realized by turning on-and-off the exchange coupling between pairs of spins. As opposed to alternate exchange-only computing schemes in which the exchange coupling acting between certain spins is always turned on [7–16], in the present computing scheme this coupling is assumed to be completely off unless it is being pulsed. Reference [6] provided the first explicit exchange-pulse sequences forming a universal gate set consisting of arbitrary single-qubit rotations and a Controlled-NOT (CNOT) gate (see also Ref. [17]).

After the first demonstration of coherent control of the exchange interaction in a semiconductor double quantum

dot [18], there have been numerous advances in fabricating and operating quantum dot systems for triple-spin qubits [19–28]. Among these experiments are many realizations of the particular kind of exchange-only qubit considered here [19–21, 24, 25], including a recent demonstration of a single-qubit device with average gate errors of 0.35% [28].

For exchange-only quantum computation with exchange pulses, single-qubit rotations are conceptually easy to obtain, requiring at most four pulses for an arbitrary rotation about the Bloch sphere [6]. The construction of two-qubit gates is significantly more complicated. This is because inter-qubit pulses, which act on spins that belong to different qubits, cause leakage out of the encoded qubit space, while any pulse sequence resulting in a logical gate needs to maintain the qubit encoding. Given the large search space for unitary operators acting on six spins, the necessity of such inter-qubit pulses greatly complicates the problem of finding pulse sequences for entangling two-qubit gates. Indeed, most such sequences have first been found through numerical searches [6, 29–31], among which is the optimal known two-qubit sequence found by Fong and Wandzura, which results in a CNOT gate [30, 32]. Recently, we provided a straightforward, analytic derivation of the Fong-Wandzura pulse sequence [33].

The first two-qubit gate sequences that have originally been constructed in analytic fashion are those presented in Ref. [34]. These sequences can be used to directly carry out an arbitrary Controlled-PHASE (CPHASE) gate which, when acting on two qubits with state labels $a = 0$ or 1 and $b = 0$ or 1, is defined as applying the identity to the two-qubit states with $ab = 00, 01$ and 10 while multiplying the $ab = 11$ state by a phase factor of $e^{i\phi}$ for some phase ϕ . Note that such CPHASE gates with $\phi = 2\pi/2^k$ for positive integer k are used in the stan-

dard implementation of the quantum Fourier transform (see, e.g., Sec. 5.1 in Ref. [35]). As opposed to the pulse sequences mentioned above [6, 29–31], the sequences of Ref. [34] have a built-in degree of freedom which allows one to directly carry out arbitrary CPHASE gates.

Recently, another set of pulse sequences for CNOT has been constructed using analytic tools rather than brute force search [36]. A crucial idea in this interesting development is to simplify the search for two-qubit sequences by allowing for leakage out of the encoded Hilbert space. The amount of leakage is then systematically suppressed by iteratively projecting these operations onto the computational Hilbert space, with every subsequent iteration reducing the amount of leakage while increasing the length of the pulse sequence. Under certain assumptions, some of the sequences presented in Ref. [36] have even shorter total duration (though comprising more clock cycles) than the Fong-Wandzura sequence.

In this paper we show how the insights gained in our earlier work on deriving two-qubit gate sequences [33, 34] can be used to analytically construct related, though more efficient, pulse sequences resulting in controlled-rotation gates locally equivalent to arbitrary CPHASE. These new sequences, similar to those of Ref. [34], contain a small number of two or three exchange pulses whose durations can be adjusted in order to choose the phase ϕ of the CPHASE gate. The arbitrary CPHASE sequences presented here, in contrast to those of Ref. [34], consist of only a few more pulses than the Fong-Wandzura CNOT sequence [30]. It is in this sense that we refer to them as efficient.

This paper is organized as follows. Section II discusses some of the basic tools and notation used below to analytically construct two-qubit pulse sequences. In Sec. III, we present a two-qubit gate construction that generalizes our derivation of the Fong-Wandzura sequence [33]. Next, in Sec. IV we design two-qubit gates by way of refining an earlier construction presented in Ref. [34]. Explicit example pulse sequences for each construction are given in Sec. V, and we conclude in Sec. VI. The equivalence of the two different representations of the Fong-Wandzura sequence given in Refs. [30] and [33] is shown explicitly in Appendix A. Appendices B to D provide various supporting explanations and calculations.

II. ROTATIONAL SYMMETRY

In this work we specify states of multiple spins using only total-spin quantum numbers. We are allowed to do so because the isotropic Heisenberg exchange Hamiltonian $J\mathbf{S}_i \cdot \mathbf{S}_j$, the only resource for realizing quantum gates considered here, is rotationally invariant.

Figure 1 shows the three-spin qubit encoding of Ref. [6] in a convenient notation (introduced to the present context in Ref. [34]) in which spins are enclosed by ovals labeled by the total spin of all particles inside. In this qubit encoding, which we adopt in our work, qubits are

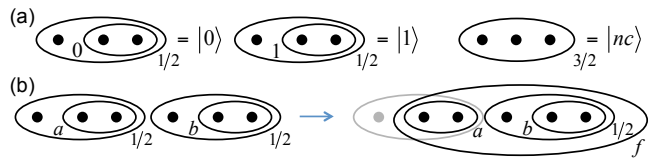


FIG. 1. Various multi-spin states given in a notation in which spin- $\frac{1}{2}$ particles, represented by \bullet , are enclosed by ovals labeled by total spin. (a) Three-spin qubit encoding of Ref. [6] showing the logical $|0\rangle$ and $|1\rangle$ states, together with the non-computational state, $|nc\rangle$. (b) A pair of three-spin qubits with state labels a and b , highlighting the five rightmost spins with total spin $f = \frac{1}{2}$ or $\frac{3}{2}$ (but not $\frac{5}{2}$, because the rightmost three spins are initialized with total spin $\frac{1}{2}$) acted on by the two-qubit pulse sequences constructed in this paper.

represented by three spins with total spin $\frac{1}{2}$, and the total spin of the rightmost two particles defines the state of the qubit. In the text a spin- $\frac{1}{2}$ is represented by the symbol \bullet , and spins are enclosed by parentheses labeled by total spin. For instance, the three-spin qubit basis states shown in Fig. 1(a) are written in the text as $|a\rangle = (\bullet(\bullet\bullet)_a)_{1/2}$ with $a = 0$ or 1 defining the standard qubit basis. Spin states—ordered top to bottom in all following figures—are ordered left to right in the text. Figure 1(a) also shows the non-computational three-spin state denoted by $|nc\rangle$, which has total spin $\frac{3}{2}$. Note that we treat a state like $(\bullet(\bullet\bullet)_a)_{1/2}$ as a single state in Hilbert space even though it is two-fold degenerate taking into account S_z quantum numbers.

Suppose that we pulse the exchange Hamiltonian $H = J(\mathbf{S}_i \cdot \mathbf{S}_j + \frac{3}{4})$ acting on two spins. In the basis $(\bullet\bullet)_a$ with state ordering $a = \{0, 1\}$, the matrix representation of the time evolution operator of such a pulse, $U_{ij}(t)$ with dimensionless time $t \in [0, 2]$, where we work in units with $\pi/J = 1$ so that $t = 1$ corresponds to a SWAP pulse ($\hbar = 1$), is then given by

$$U_{ij}(t) = \text{diag}(1, e^{-i\pi t}) \quad (1)$$

$$= e^{-i\pi t/2} e^{i\pi t \hat{\mathbf{z}} \cdot \boldsymbol{\sigma}/2}. \quad (2)$$

Here, $\boldsymbol{\sigma} = (\sigma_x, \sigma_y, \sigma_z)$ denotes the Pauli matrix vector. The inverse of an exchange pulse of duration t is a pulse of duration $s = 2 - t$. We will often use the fact that, if we take the states $(\bullet\bullet)_0$ and $(\bullet\bullet)_1$ as the up and down states of a pseudospin, Eq. (2) can be interpreted as a z -axis pseudospin rotation through positive angle πt .

Below we construct sequences of exchange pulses, which are described by time evolution operators of the type of Eq. (1), for carrying out entangling two-qubit gates. As pointed out above, finding such a two-qubit sequence is nontrivial because pulse sequences acting on two qubits do not, in general, maintain the qubit encoding. To be specific, consider the two three-spin qubits shown on the left-hand side (LHS) of Fig. 1(b). Notice that exchange pulses applied to spins within a qubit leave its total spin invariant, whereas a pulse acting on the two central spins (i.e., the rightmost spin of the left qubit and

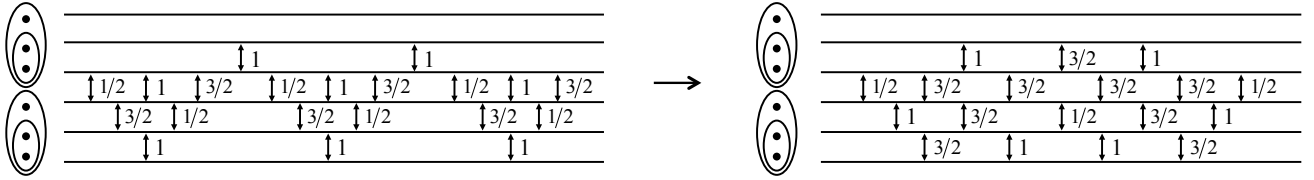


FIG. 2. Two equivalent representations of the Fong-Wandzura pulse sequence. In Appendix A it is shown explicitly how the sequence on the LHS, derived in Ref. [33], can be turned into the sequence on the RHS, obtained numerically in Ref. [30] (given here up to single-qubit rotations).

the leftmost spin of the right qubit) alters the total spin of each qubit and therefore results in leakage out of the computational space.

The two-qubit gate sequences presented below can be applied to only five of the six spins encoding two qubits, which can be chosen to be those five spins highlighted in Fig. 1(b). As shown in Ref. [34], any pulse sequence that acts on only five spins and carries out a leakage-free two-qubit gate for total spin 1 of the two logical qubits results in the very same gate for total spin 0. In contrast, when applying the original CNOT sequence found by Di-Vincenzo et al. [6] to the qubits shown on the LHS of Fig. 1(b), all six spins undergo nontrivial exchange pulses (i.e., pulses different from SWAP), and a CNOT gate is carried out only for total spin 1.

III. GENERALIZING THE DERIVATION OF THE FONG-WANDZURA SEQUENCE

In this section we construct a family of two-qubit gate sequences whose derivation can be understood as a generalization of the derivation of the Fong-Wandzura pulse sequence presented in Ref. [33]. It is thus worthwhile reviewing some of the main steps of that derivation. In doing this, we take the Fong-Wandzura sequence as a starting point and imagine “reverse engineering” it to reveal its fundamental structure, and then show how this structure can be altered to find new two-qubit gate sequences. We note that the order of ideas presented in this review is the reverse of that of [33], where the Fong-Wandzura sequence was constructed essentially from the bottom up.

The derivation given in Ref. [33] is based on the observation that the pulses of the Fong-Wandzura sequence as published in Ref. [30] can be rearranged without changing the unitary operation carried out by this sequence so that it consists of recurring patterns of a smaller pulse sequence. This fact is illustrated in Fig. 2, where we show two different representations of the Fong-Wandzura sequence acting on two encoded three-spin qubits. The LHS of Fig. 2 shows a pulse sequence, which has been analytically derived in Ref. [33] as an equivalent representation of the originally published version of the Fong-Wandzura sequence [30], which, upon removing four pulses used for single-qubit rotations, is shown on the

RHS of the same figure. In Appendix A it is shown explicitly how the sequences of Fig. 2 can be turned into one another (up to a single-qubit SWAP pulse not shown in this figure) using only a small set of elementary manipulations, such as moving SWAP pulses past other pulses, or combining neighboring pulses that act on the same pair of spins to single pulses.

Figure 3 summarizes a crucial step of the analytic derivation of the Fong-Wandzura sequence [33]. This step is based on the observation that the pulse sequence on the LHS of Fig. 2 exhibits three repeated patterns of a six-pulse sequence, each of which acts on the lowermost four spins and comprises two SWAPs, two $\sqrt{\text{SWAPs}}$ and two inverse $\sqrt{\text{SWAPs}}$. In Fig. 3(a) we consider the lowermost five spins that the Fong-Wandzura sequence explicitly acts on, which are the same five spins as those highlighted in Fig. 1(b), and substitute the qubit with state label b by a symbol \star . We then apply the sequence shown on the LHS of Fig. 2 to these spins, where each repeated six-pulse sequence is denoted by R . Figure 3(a) also shows the matrix representation of the unitary operation due to this sequence [33] in the six-dimensional Hilbert space spanned by the basis states $((\bullet\bullet)_a(\bullet(\bullet\bullet)_b)_{1/2})_f$ with $ab = 00, 01, 10$ and 11 if $f = \frac{1}{2}$ and $ab = 10$ and 11 if $f = \frac{3}{2}$. Note that when replacing three spins with total spin $\frac{1}{2}$ as in Fig. 3(a),

$$(\bullet(\bullet\bullet)_b)_{1/2} \rightarrow \star, \quad (3)$$

the quantum number b is suppressed. For the state labeling corresponding to the basis of the matrix shown in Fig. 3(a) this implies

$$\begin{aligned} abf &= \{00\frac{1}{2}, 01\frac{1}{2}, 10\frac{1}{2}, 11\frac{1}{2} | 10\frac{3}{2}, 11\frac{3}{2}\} \\ &\xrightarrow{(3)} af = \{\mathbf{0}\frac{1}{2}, \mathbf{1}\frac{1}{2} | \mathbf{1}\frac{3}{2}\}, \quad (4) \end{aligned}$$

because of which the matrix elements of the matrix in Fig. 3(a) are 2×2 block elements, rather than numbers, which act on the two-dimensional qubit space hidden inside \star . [Two-dimensional basis states, such as those on the right-hand side of Eq. (4), are shown in bold print.] In order for this pulse sequence to have a matrix representation consisting entirely of unitary 2×2 blocks, its operation is required to conserve the total spin of the qubit represented by \star . In fact, we place this very re-

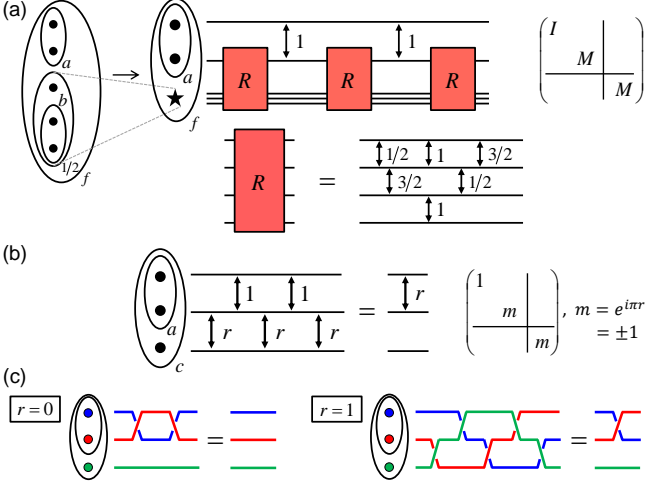


FIG. 3. (Color online) Crucial step in our derivation of the Fong-Wandzura sequence [33]. (a) The Fong-Wandzura sequence, as given on the LHS of Fig. 2, applied to the five spins highlighted in Fig. 1(b), together with its matrix representation in the effective basis (4) with $M = \hat{n}_0 \cdot \boldsymbol{\sigma}$. The lowermost three spins are represented by an effective spin- $\frac{1}{2}$ particle, \star , and R represents the repeated six-pulse sequence. (b) Simple three-spin sequence consisting of three r -pulses and two explicit SWAPs, which is used to deduce crucial properties of the sequence in (a). (c) Graphical evaluation of the sequence shown in (b) for the cases $r = 0$ and 1 , where SWAP pulses are represented by particle exchanges. As described in the text, we use (c) to show that the sequence in (b) is, in both cases, equivalent to an r -pulse applied to the top two spins. In (b) we also show the matrix representation of this r -pulse in the basis $ac = \{0 \frac{1}{2}, 1 \frac{1}{2} | 1 \frac{3}{2}\}$.

quirement on all pulse sequences constructed below that act on a number of spins including \star .

Given the matrix shown in Fig. 3(a) in the af -basis (4), the operation carried out by the two-qubit sequence shown in this figure applies the 2×2 identity, $\mathbb{1}$, if $a = 0$, and the 2×2 matrix $M = \hat{n}_0 \cdot \boldsymbol{\sigma}$ [33] if $a = 1$, regardless of the value of f ; here \hat{n}_0 is a three-dimensional unit vector [37]. Accordingly, in the two-qubit basis $ab = \{00, 01, 10, 11\}$ the matrix of the gate carried out by this sequence is

$$U_{FW} = \text{diag}(\mathbb{1}, M). \quad (5)$$

With $M = \hat{n}_0 \cdot \boldsymbol{\sigma}$ this gate is locally equivalent to CNOT.

In Ref. [33], the two-qubit sequence of Fig. 3(a) was viewed as an elevated version of the simpler sequence shown in Fig. 3(b). This simpler sequence consists of explicit SWAPs and pulses of duration $r = 0$ or 1 , which we denote as r -pulses. According to Eq. (1), the matrix representation of an r -pulse acting on two spins in the basis $(\bullet\bullet)_a$ with state ordering $a = \{0, 1\}$ is

$$U_r = \text{diag}(1, e^{-i\pi r}) = \text{diag}(1, m), \quad m^2 = 1. \quad (6)$$

If $r = 0$ then $m = 1$ and the r -pulse carries out the identity operation. If $r = 1$ then $m = -1$ and the r -pulse carries out a SWAP. Note that the sequence in Fig. 3(a) can

be obtained by replacing the lowermost spin in Fig. 3(b) with an effective spin- $\frac{1}{2}$ particle, \star , and further replacing each r -pulse with an \bar{R} sequence.

The pulse sequence shown in Fig. 3(b) can be evaluated straightforwardly, because all its pulses are equivalent to simple particle permutations (the identity for $r = 0$ and SWAP for $r = 1$). This evaluation is illustrated in Fig. 3(c). There are two cases to consider, $r = 0$ and $r = 1$. For the $r = 0$ sequence, the three r -pulses can be removed to obtain two consecutive SWAPs that cancel one another. For the $r = 1$ sequence, tracing each particle line through the diagram results in a net exchange of only the top two particles. These two cases are thus correctly combined in Fig. 3(b), where this five-pulse sequence is shown as being equivalent to a single r -pulse applied to the top two spins. The corresponding matrix representation, shown in Fig. 3(b), can be directly read off Eq. (6).

The matrix representation of an initially generic R sequence in the basis $(\bullet\star)_d$ with state ordering $d = \{0, 1\}$, is [33]

$$R = \text{diag}(\mathbb{1}, M), \quad M^2 = \mathbb{1}. \quad (7)$$

Here, the requirement $M^2 = \mathbb{1}$ is an elevated version of the requirement $m^2 = 1$ in Eq. (6), and is needed for the R sequence to be viewed as an elevated r -pulse. For the one-dimensional case the equation $m^2 = 1$ has the two solutions $m = \pm 1$. In contrast, the equation $M^2 = \mathbb{1}$ has, in addition to the equivalent solutions $M = \pm \mathbb{1}$, a continuum of solutions, $M = \hat{n} \cdot \boldsymbol{\sigma}$, where \hat{n} can be any unit vector. Finally, as discussed in Ref. [33], by elevating the simple pulse sequence of Fig. 3(b) to that of Fig. 3(a), one can directly infer the matrix representation of the Fong-Wandzura sequence shown in Fig. 3(a).

We now turn to our new pulse sequence construction, which is based on the insights gained through the reverse engineering process described above. Consider the sequence of spin permutations and one exchange pulse of arbitrary duration t , or t -pulse, shown on the LHS of Fig. 4(a). Clearly, an equivalent way to represent this sequence is to only apply the t -pulse to the top two spins. Replacing all these particle exchanges with SWAPs yields the pulse sequence shown on the LHS of Fig. 4(b), which, using the identity of (a), is found to be equivalent to the single t -pulse applied to the top two spins. The matrix representation of the sequence shown in Fig. 4(b) can thus be directly read off Eq. (1).

In a similar way as the two-qubit pulse sequence shown in Fig. 3(a) can be interpreted as a generalization of the sequence in Fig. 3(b), we now generalize the sequence shown in Fig. 4(b) to the two-qubit sequence in Fig. 4(c). This last sequence is applied to the five spins highlighted in Fig. 1(b) upon representing the qubit with state label b by an effective spin- $\frac{1}{2}$, \star . The schematic operations T and S can be viewed as elevated versions of t -pulse and a SWAP, respectively, and are realized by pulse sequences—to be determined—which are applied to one spin- $\frac{1}{2}$, \bullet , and the three spins inside the effective spin- $\frac{1}{2}$,

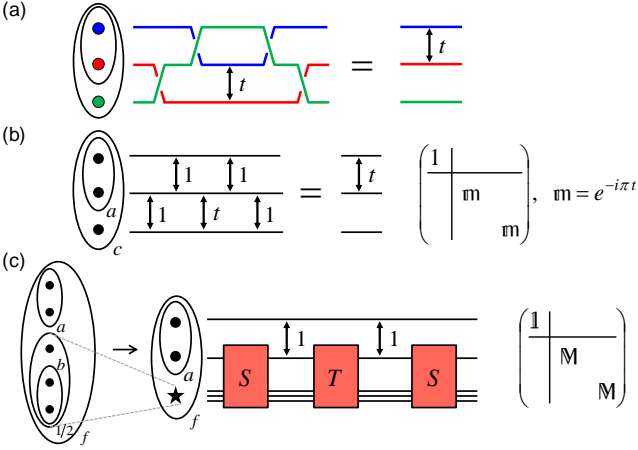


FIG. 4. (Color Online) Two-qubit gate construction generalizing that shown in Fig. 3, with steps in reverse order. (a) Sequence of particle interchanges and a t -pulse. It is readily seen that this sequence is equivalent to only applying the t -pulse to the top two spins. (b) Sequence of four SWAPS and one t -pulse, which is simplified using (a) by interpreting SWAPS as particle interchanges. Its corresponding matrix representation is shown in the indicated basis with $ac = \{0\frac{1}{2}, 1\frac{1}{2}|1\frac{3}{2}\}$. (c) Two-qubit sequence, which is an elevated version of the sequence shown in (b), applied to the five spins highlighted in Fig. 1(b). The lower qubit with state label b is represented by an effective spin- $\frac{1}{2}$, \star . The corresponding matrix with arbitrary \mathbb{M} is given in the effective basis (4), i.e., $a\mathbb{f} = \{0\frac{1}{2}, 1\frac{1}{2}|1\frac{3}{2}\}$.

★. Note that the effective Hilbert space of these particles is spanned by the states $(\bullet\star)_d$ with $d = 0$ or 1 , but not 2 because the total spin of the qubit hidden inside \star , as given in Eq. (3), is initialized to be $\frac{1}{2}$.

The t -pulse, whose matrix representation is shown in Fig. 4(b), is generalized to the T operation by promoting the numbers 1 and $\mathbb{m} = e^{-i\pi t}$ to the unitary 2×2 matrices $\mathbb{1}$ and \mathbb{M} , respectively. As opposed to the matrix M introduced above, the matrix \mathbb{M} is not required to fulfill any special condition (besides being unitary). The matrix representation of the operation carried out by T when applied as in Fig. 4(c) in the basis $(\bullet\star)_d$ with $d = \{0, 1\}$ is then

$$T = \text{diag}(\mathbb{1}, \mathbb{M}). \quad (8)$$

A SWAP operation, whose matrix is given by Eq. (6) for the case of $m = -1$, is similarly generalized to the S operation by promoting the numbers ± 1 to the 2×2 matrices $\pm \mathbb{1}$, respectively. Accordingly, the matrix corresponding to the S -operation when applied to \bullet and \star as in Fig. 4(c) in the basis $(\bullet\star)_d$ with $d = \{0, 1\}$ is

$$S = \text{diag}(\mathbb{1}, -\mathbb{1}). \quad (9)$$

The matrix representation of the two-qubit sequence shown in Fig. 4(c) consists of 2×2 block elements that act on the Hilbert space of the qubit hidden inside the effective spin- $\frac{1}{2}$, \star , because the operations T , S and SWAP

conserve this qubit's total spin. To find this matrix representation, we first note that each of its 2×2 block elements must be a polynomial linear in \mathbb{M} , $\alpha_0\mathbb{1} + \alpha_1\mathbb{M}$, because there is only one operation in this sequence, T , whose matrix contains an element unequal to $\pm \mathbb{1}$, namely \mathbb{M} . These polynomials are determined for any \mathbb{M} by the special case of $\mathbb{M} = e^{-i\pi t}\mathbb{1}$, for which the sequence shown in Fig. 4(c) is equivalent to that shown in Fig. 4(b). Accordingly, the matrix shown in Fig. 4(c) is an elevated version of that shown in Fig. 4(b).

When applying the pulse sequence of Fig. 4(c) to the qubits shown in Fig. 1(b), we can deduce its action by noting that its matrix representation in the basis (4) is the identity for $a = 0$, and \mathbb{M} for $a = 1$ (independent of f). This corresponds to the quantum gate

$$U_{2\text{qubit}} = \text{diag}(\mathbb{1}, \mathbb{M}). \quad (10)$$

The sequence of Fig. 4(c) may thus be used to carry out an arbitrary controlled-operation gate with the control and target being the qubits with state labels a and b , respectively. For the parameterization

$$\mathbb{M}(\phi) = e^{i\xi} e^{i\phi \hat{\mathbf{n}} \cdot \boldsymbol{\sigma}/2} \quad (11)$$

the two-qubit gate (10) is then a controlled-rotation gate with angle ϕ and axis $\hat{\mathbf{n}}$ and an additional phase ξ . Here we write $\mathbb{M} = \mathbb{M}(\phi)$, since ϕ is the only parameter invariant under single-qubit rotations.

In principle, one can use any four-spin pulse sequences satisfying Eqs. (8) and (9) for the operations T and S , which have been left implicit up to now. Since Eq. (10) is a function of \mathbb{M} only, the actual two-qubit gate then only depends on the particular realization of the T sequence. In Appendix B we derive an explicit set of pulse sequences for T and S . In doing this, we combine insights gained by deriving the Fong-Wandzura sequence [33] with tools from Ref. [34]. The resulting set of two-qubit gate sequences is given in Sec. V.

IV. OPTIMIZED CPHASE GATES

We now present an analytic two-qubit gate construction based on a set of tools and concepts developed previously for constructing pulse sequences for arbitrary CPHASE gates [34]. The resulting sequences carry out the same two-qubit gates using fewer exchange pulses.

Figure 5 shows the three basic pulse sequences used in this construction, U_3 , \bar{U}_3 , and U_4 . Consider the three spin- $\frac{1}{2}$ particles shown in Fig. 5(a), whose three-dimensional Hilbert space is spanned by the states $((\bullet\bullet)_a\bullet)_c$ with quantum numbers $ac = 0\frac{1}{2}, 1\frac{1}{2}$ and $1\frac{3}{2}$. The first building block for our two-qubit gate construction is the operation U_3 shown in Fig. 5(a), which was introduced in Ref. [34]. The pulses making up U_3 are of durations t and \bar{t} with $0 \leq t \leq \bar{t} \leq 2$, which fulfill

$$\tan(\pi t/2) \tan(\pi \bar{t}/2) = -2. \quad (12)$$

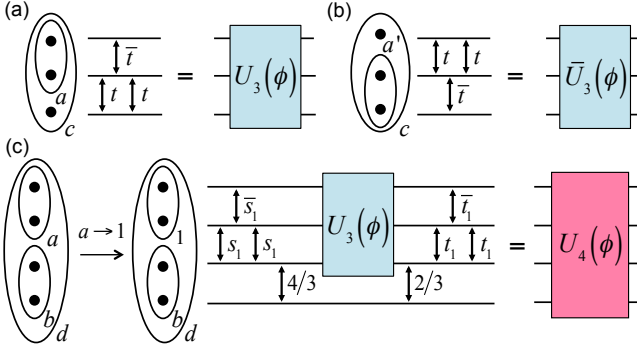


FIG. 5. Pulse sequences adapted from Ref. [34] carrying out operations serving as building blocks for our two-qubit gate construction. (a) Operation U_3 , whose matrix representation is given by Eq. (13) in the indicated ac -basis. (b) Operation \bar{U}_3 , whose matrix representation (15) is given in the indicated a' - c -basis. The parameters t , \bar{t} and ϕ shown in both (a) and (b) are related to one another via Eqs. (12) and (14). (c) Operation U_4 , whose matrix representation (17) is given in the indicated bd -basis. Here, the explicit t_1 , \bar{t}_1 , t_1 and s_1 , \bar{s}_1 , s_1 sequences carry out $U_3(2\pi/3)$ and $U_3(4\pi/3)$ operations, respectively. By solving Eqs. (12) and (14) for $\phi = 2\pi/3$, one finds $t_1 = 0.426548$ [34]. The values of \bar{t}_1 , s_1 and \bar{s}_1 are then determined by Eq. (12) and the relation $t_1 + s_1 = \bar{t}_1 + \bar{s}_1 = 2$ which follows from the fact that $4\pi/3 = 2\pi - 2\pi/3$ (see main text).

As discussed in Ref. [34], the matrix representation of the operation U_3 in the ac -basis shown in Fig. 5(a) with state ordering $ac = \{0\frac{1}{2}|1\frac{1}{2}, 1\frac{3}{2}\}$ is

$$U_3(\phi) = \begin{pmatrix} e^{-i\pi\bar{t}} & & \\ & 1 & \\ & & e^{-i\phi} \end{pmatrix}, \quad (13)$$

where

$$\phi = \pi(t + \bar{t} - 1), \quad \phi \in [0, 2\pi]. \quad (14)$$

As indicated by the solid lines in Eq. (13), the operation U_3 conserves the total spin of the top two particles (denoted a) shown in Fig. 5(a). Note that U_3 acts trivially on the one-dimensional $a = 0$ subspace, i.e., here it is proportional to the identity, while it applies a phase shift of $e^{-i\phi}$ between the $a = 1$ states with $c = \frac{1}{2}$ and $\frac{3}{2}$.

The pulse sequence for \bar{U}_3 is shown in Fig. 5(b). Since this sequence is the mirror image of the U_3 sequence in Fig. 5(a), we can directly infer the matrix representation of \bar{U}_3 in the mirrored basis $(\bullet(\bullet\bullet)_{a'})_c$ to be simply that given in Eq. (13). Therefore, in the basis $a'c = \{0\frac{1}{2}|1\frac{1}{2}, 1\frac{3}{2}\}$ we find

$$\bar{U}_3(\phi) = \begin{pmatrix} e^{-i\pi\bar{t}} & & \\ & 1 & \\ & & e^{-i\phi} \end{pmatrix} \quad (15)$$

with t , \bar{t} and ϕ related to one another via Eqs. (12) and (14). As opposed to the operation U_3 , this mirrored op-

eration \bar{U}_3 conserves the total spin of the lower two spins shown in Fig. 5(b) (denoted a'), and applies a phase shift of $e^{-i\phi}$ between the $a' = 1$ states while it acts trivially if $a' = 0$.

The inverse of a t , \bar{t} , t sequence shown in Fig. 5(a), which carries out the operation $U_3(\phi)$, is the same three-pulse sequence with inverted durations s , \bar{s} , s , where $s = 2 - t$ and $\bar{s} = 2 - \bar{t}$ (note that $s \geq \bar{s}$ since $t \leq \bar{t}$). We denote the corresponding operation $U_3(\chi)$, and we take from Eq. (14) that indeed $\chi = \pi(s + \bar{s} - 1) = 2\pi - \phi$. Similarly, the inverse of the $\bar{U}_3(\phi)$ operation, whose t , \bar{t} , t sequence is shown in Fig. 5(b), is the same sequence with inverted durations s , \bar{s} , s , which carries out the operation $\bar{U}_3(\chi)$ with the same s , \bar{s} and χ as those for $U_3(\chi)$. The matrix representations of $U_3(\chi)$ and $\bar{U}_3(\chi)$ are, respectively, given by Eqs. (13) and (15) in the indicated bases, upon replacing $\phi \rightarrow \chi$ and $\bar{t} \rightarrow \bar{s}$.

Finally, Fig. 5(c) shows the third sequence, U_4 , which is applied to four spins. The Hilbert space of these spins is six-dimensional. For the indicated basis, $((\bullet\bullet)_a(\bullet\bullet)_b)_d$, the $d = 0$ space is spanned by the states with $ab = 00$ and 11 , the $d = 1$ space by the states with $ab = 01, 10$ and 11 , and the $d = 2$ space by the $ab = 11$ state. As shown in the figure, the pulse sequence of U_4 consists of a number of pulses of fixed durations, independent of ϕ , together with a $U_3(\phi)$ sequence [see Fig. 5(a)].

The operation U_4 was designed in Ref. [34] to apply a simple phase factor to all $a = 0$ states $((\bullet\bullet)_a=0(\bullet\bullet)_b)_{d=b}$,

$$U_4(\phi) = e^{-i\pi\bar{t}} \mathbb{1}, \quad (a = 0). \quad (16)$$

As indicated in Fig. 5(c), we therefore concentrate on the four-dimensional $a = 1$ Hilbert space, which is spanned by the states $((\bullet\bullet)_{a=1}(\bullet\bullet)_b)_d$ with $bd = 10, 01, 11$ and 12 . In the basis $bd = \{10|01|11, 12\}$ the operation U_4 has the matrix representation

$$U_4(\phi) = \begin{pmatrix} 1 & & & \\ & 1 & & \\ & & e^{-i\phi} & \\ & & & e^{-i\phi} \end{pmatrix}. \quad (17)$$

In this matrix, solid lines separate out the one-dimensional $b = 0$ sector where U_4 acts as the identity. U_4 thus acts trivially for both of the cases $a = 0$ or $b = 0$.

Note all three sequences shown in Fig. 5 act in a simple way. They (i) conserve the total-spin quantum numbers of certain spin pairs, and (ii) act trivially [i.e., proportional to the identity] only if those quantum numbers are equal to 0.

To design two-qubit gates, we consider the five spins highlighted in Fig. 1(b),

$$((\bullet\bullet)_a(\bullet(\bullet\bullet)_b)_c)_f, \quad (18)$$

where $a, b = 0$ or 1 define the states of the two logical qubits, and $c, f = \frac{1}{2}$ or $\frac{3}{2}$. As opposed to Fig. 1(b), here we take the case of $c = \frac{3}{2}$ into account because, as explained in Sec. II, the total spin of a logical qubit,

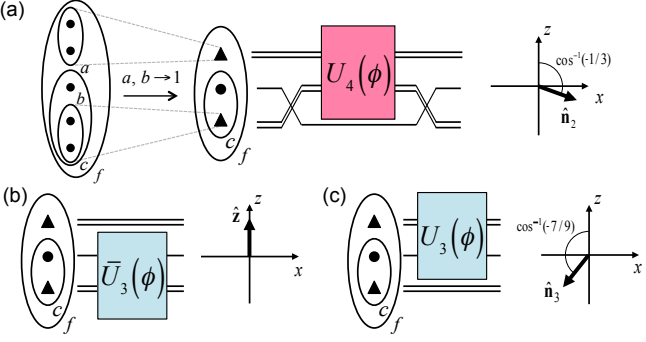


FIG. 6. Operations U_4 , \bar{U}_3 and U_3 applied to the five spins highlighted in Fig. 1(b). Each operation acts trivially if the total spin of the topmost or lowermost two particles is 0. We thus work in an effective Hilbert space by setting both a and b to 1, as indicated by the symbols \blacktriangle [see Eq. (20)]. The U_4 operation in (a) is surrounded by generalized SWAPS, which ensure that the U_4 sequence is applied to the spin pairs with total spins a and b . Each operation carries out a pseudospin rotation on $\{\uparrow_{1/2}, \downarrow_{1/2}\}$ defined in Eq. (24) about the indicated axes \hat{n}_2 [for U_4 as shown in (a)], \hat{z} [for \bar{U}_3 in (b)] and \hat{n}_3 [for U_3 in (c)].

which is initialized to be $\frac{1}{2}$, is altered by certain exchange pulses.

Figure 6 shows how we apply the operations of Fig. 5 to the spins (18). This particular layout takes full advantage of the spin-conservation feature summarized above, since each of the three operations conserves the quantum numbers a and b . From the discussion above, this conservation is easy to see for the operations U_3 and \bar{U}_3 . The U_4 operation shown in Fig. 6(a), however, is defined in Fig. 5(c) as acting on two neighboring spin pairs with total spins a and b . To ensure the conservation of a and b , it is thus sandwiched between generalized SWAPS that interchange the spin \bullet with the spin pair $(\bullet\bullet)_b$.

We now concatenate the operations shown in Fig. 6 to design arbitrary CPHASE gates of the form

$$U_{\text{CPHASE}}(\phi) = \text{diag}(1, 1, 1, e^{-i\phi}) \quad (19)$$

in the two-qubit basis $ab = \{00, 01, 10, 11\}$. As explained in Appendix C1, the operations of Fig. 6 result in simple phase factors if $a = 0$ or $b = 0$, which only depend on the state of one of the qubits and can therefore be undone by single-qubit rotations before or after the main two-qubit gate sequence. We can therefore focus on the nontrivial, effective Hilbert space spanned by states (18) with $ab = 11$. As also shown in Fig. 6(a), this effective space is obtained by replacing those spin pairs with total spin 1 by effective spin-1 particles denoted \blacktriangle ,

$$(\bullet\bullet)_1 \rightarrow \blacktriangle, \quad (20)$$

$$((\bullet\bullet)_{a=1} (\bullet(\bullet\bullet)_{b=1})_c)_f \rightarrow (\blacktriangle(\bullet\blacktriangle)_c)_f. \quad (21)$$

The corresponding four-dimensional Hilbert space is spanned by the states with $cf = \frac{1}{2}\frac{1}{2}, \frac{3}{2}\frac{1}{2}, \frac{1}{2}\frac{3}{2}$ and $\frac{3}{2}\frac{3}{2}$.

Figure 7 shows both the original pulse sequence presented in Ref. [34] (top panel, operation \bar{U}_5) as well as the

new sequence developed here (bottom panel, operation U_5). [We note that the \bar{U}_5 sequence is a slightly altered version of that published in Ref. [34] due to a different choice of qubit bases.] As shown on the right side of the figure, applying the sequences \bar{U}_5 and U_5 to two encoded three-spin qubits enacts an arbitrary CPHASE gate up to the indicated single-qubit rotations. Note that, qualitatively speaking, the new sequence for U_5 is the same as that for \bar{U}_5 upon replacing the outer U_4 operations by U_3 operations. This is why these new sequences contain fewer exchange pulses than those originally published in Ref. [34].

We now explain how the two CPHASE gate sequences shown in Fig. 7 can be derived analytically based on geometric intuition. Our derivation is based on the fact that both $\bar{U}_5(\phi) = U_4(\chi_1)\bar{U}_3(\phi_1)U_4(\phi)\bar{U}_3(\chi_1)U_4(\phi_1)$ and $U_5(\phi) = U_3(\phi_3)\bar{U}_3(\phi_2)U_4(\phi)\bar{U}_3(\chi_2)U_3(\chi_3)$ with $\chi_i = 2\pi - \phi_i$ for $i = 1, 2, 3$ can be understood in terms of similarity transformations. [Here and below the operations U_3 , \bar{U}_3 , and U_4 are understood to be acting on the full five-spin Hilbert space as shown Fig. 6.] To see the similarity transformation structure, note that $\chi_1 = 2\pi - \phi_1$ implies $\bar{U}_3(\chi_1) = \bar{U}_3(\phi_1)^{-1}$ and $U_4(\chi_1) = U_4(\phi_1)^{-1}$, so that we can write

$$\bar{U}_5(\phi) = PU_4(\phi)P^{-1}, \quad P = U_4(\chi_1)\bar{U}_3(\phi_1). \quad (22)$$

Similarly, $\chi_{2,3} = 2\pi - \phi_{2,3}$ implies $\bar{U}_3(\chi_2) = \bar{U}_3(\phi_2)^{-1}$ and $U_3(\chi_3) = U_3(\phi_3)^{-1}$, so that

$$U_5(\phi) = QU_4(\phi)Q^{-1}, \quad Q = U_3(\phi_3)\bar{U}_3(\phi_2). \quad (23)$$

Since each operation in Eqs. (22) and (23) is of the form of a similarity transformation, any phases applied by P or Q on the $a = 0$ or $b = 0$ subspace cancel out, since here U_4 acts proportional to the identity. For this subspace, the only nonzero phase applied by either U_5 or \bar{U}_5 is then that due to $U_4(\phi)$ for $a = 0$. According to Eq. (16) this phase factor is $e^{-i\pi\bar{t}}$, and for each sequence it is undone by a corresponding single-qubit pulse of duration \bar{t} applied to the spin pair $(\bullet\bullet)_a$, as shown to the far right in Fig. 7 [compare Fig. 1(b)].

In order to understand how the operations shown in Fig. 6 act on the $ab = 11$ Hilbert space spanned by the states (21), we introduce a pseudospin

$$\uparrow_f = (\blacktriangle(\bullet\blacktriangle)_{1/2})_f, \quad \downarrow_f = (\blacktriangle(\bullet\blacktriangle)_{3/2})_f, \quad (24)$$

for both the $f = \frac{1}{2}$ and $\frac{3}{2}$ sectors. The actions of U_3 , \bar{U}_3 and U_4 on these pseudospin spaces are worked out in Appendix C2. Consulting Eqs. (C17) and (C15), the matrix representation of U_4 on these $f = \frac{1}{2}$ and $f = \frac{3}{2}$ pseudospins $\{\uparrow_f, \downarrow_f\}$ is

$$U_4^{f=1/2}(\phi) = e^{-i\phi/2} e^{i\phi\hat{n}_2 \cdot \sigma/2}, \quad (25)$$

$$U_4^{f=3/2}(\phi) = e^{-i\phi} \mathbb{1}. \quad (26)$$

For $f = \frac{1}{2}$, $U_4(\phi)$ is a pseudospin rotation through angle ϕ about the axis $\hat{n}_2 = (2\sqrt{2}/3, 0, -1/3)$ [38], which is

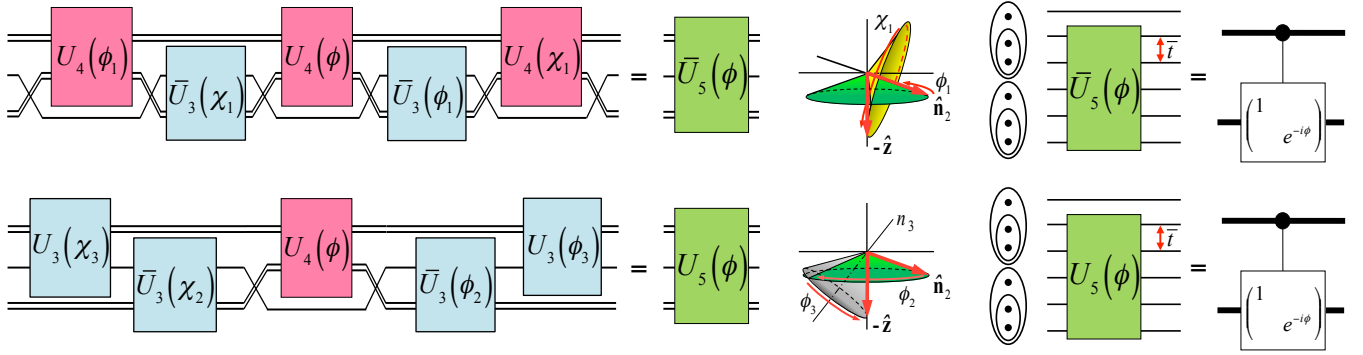


FIG. 7. (Color online) Constructing two-qubit gates applied to the five spins highlighted in Fig. 1(b). Top panel: \bar{U}_5 gate sequence of Ref. [34] consisting of three U_4 and two U_3 -like operations. Bottom panel: Optimized sequence U_5 consisting of only one U_4 and four U_3 -like operations. As also shown, \bar{U}_5 and U_5 , constructed via similarity transformations and augmented by single-qubit pulses explained in the text, can be used to carry out arbitrary CPHASE gates with $\phi \in [0, 2\pi]$. The transformation of each sequence is visualized by the respective diagram featuring two intersecting cones where $\chi_i = 2\pi - \phi_i$, and ϕ_i for $i = 1, 2, 3$ are given by Eqs. (31)-(33). Note that the cones for the top panel have undergone a π rotation about the z axis when compared to those given in Ref. [34]. This is due to the change in qubit basis which manifests itself in the six generalized SWAPS in this sequence.

indicated in Fig. 6(a). Similarly, consulting Eqs. (C18) and (C19) we have

$$\bar{U}_3(\phi) = e^{-i\phi/2} e^{i\phi\hat{\mathbf{z}} \cdot \boldsymbol{\sigma}/2}, \quad (27)$$

$$U_3(\phi) = e^{-i\phi/2} e^{i\phi\hat{\mathbf{n}}_3 \cdot \boldsymbol{\sigma}/2}, \quad (28)$$

each of which results in the same pseudospin rotation through angle ϕ in both $f = \frac{1}{2}$ and $\frac{3}{2}$ sectors. The rotation axes $\hat{\mathbf{z}}$ and $\hat{\mathbf{n}}_3 = (-\frac{4\sqrt{2}}{9}, 0, -\frac{7}{9})$ are indicated in Figs. 6(b) and (c), respectively.

For the operations \bar{U}_5 and U_5 to result in a CPHASE gate, Eq. (19) states that the $ab = 11$ two-qubit states $((\bullet\Delta)_{1/2}(\bullet\Delta)_{1/2})_g$ with $g = 0$ and 1 , obtained by combining the six-spin states in Fig. 1(b) with Eq. (20), $(\bullet\bullet)_1 \rightarrow \Delta$, need to be multiplied by $e^{i\phi}$. Expanding these two-qubit states in the basis $(\bullet(\Delta(\bullet\Delta)_{1/2})_f)_g$ yields finite overlap with both $f = \frac{1}{2}$ and $\frac{3}{2}$ states [such concrete expansions are given by Eqs. (23) and (24) in Ref. [34]]. \bar{U}_5 and U_5 must therefore multiply both pseudospin states $\uparrow_{1/2}$ and $\uparrow_{3/2}$ by the same phase factor $e^{-i\phi}$.

Note that the similarity transformations due to P and Q in Eqs. (22) and (23), respectively, have no effect on the $f = \frac{3}{2}$ pseudospin sector because here U_4 is proportional to the identity [see Eq. (26)], so that

$$\bar{U}_5^{f=3/2}(\phi) = U_5^{f=3/2}(\phi) = e^{-i\phi} \mathbb{1}. \quad (29)$$

\bar{U}_5 and U_5 thus multiply the state $\uparrow_{3/2}$ by $e^{-i\phi}$ for arbitrary P and Q . The transformations (22) and (23) must then ensure that $\uparrow_{1/2}$ is multiplied by the same phase factor. This is accomplished by mapping $\hat{\mathbf{n}}_2$, the rotation vector of U_4 , to $-\hat{\mathbf{z}}$, so that in the pseudospin basis $\{\uparrow_{1/2}, \downarrow_{1/2}\}$ we have

$$\begin{aligned} \bar{U}_5^{f=1/2}(\phi) &= U_5^{f=1/2}(\phi) = e^{-i\phi/2} e^{i\phi(-\hat{\mathbf{z}}) \cdot \boldsymbol{\sigma}/2} \\ &= \text{diag}(e^{-i\phi}, 1). \end{aligned} \quad (30)$$

The similarity transformation (22) found analytically in Ref. [34], carried out by $P = U_4(\chi_1) \bar{U}_3(\phi_1)$, is visualized by the two intersecting cones in the top panel of Fig. 7. Here the green cone is described by rotating the vector $\hat{\mathbf{n}}_2$ about the z axis, and the yellow cone by rotating the vector $-\hat{\mathbf{z}}$ about the n_2 axis. The transformation due to P then consists of a rotation of the vector $\hat{\mathbf{n}}_2$ about the z -axis through angle ϕ_1 to the intersection of the two cones, followed by a rotation about the n_2 axis through $\chi_1 = 2\pi - \phi_1$ to the negative z axis. The rotation angle is [34]

$$\phi_1 = \cos^{-1} \frac{\hat{\mathbf{n}}_2 \cdot \hat{\mathbf{z}}}{\hat{\mathbf{n}}_2 \cdot \hat{\mathbf{z}} - 1} = \cos^{-1}(1/4). \quad (31)$$

The similarity transformation (23) for U_5 , carried out by $Q = \bar{U}_3(\phi_3) U_3(\phi_2)$, is visualized by the green and gray cones shown in the lower panel of Fig. 7. Here the green cone is the same as that used before, while the gray cone is described by rotating $-\hat{\mathbf{z}}$ about the n_3 -axis. The transformation due to Q is then a rotation of $\hat{\mathbf{n}}_2$ about $\hat{\mathbf{z}}$ through angle ϕ_2 to the intersection of the cones, followed by an n_3 -axis rotation through ϕ_3 to $-\hat{\mathbf{z}}$. It is a simple exercise to show that the rotation angles are

$$\phi_2 = \cos^{-1} \left(-\frac{\hat{\mathbf{n}}_3 \cdot \hat{\mathbf{z}} (1 + \hat{\mathbf{n}}_2 \cdot \hat{\mathbf{z}})}{(\hat{\mathbf{n}}_2 \cdot \hat{\mathbf{x}})(\hat{\mathbf{n}}_3 \cdot \hat{\mathbf{x}})} \right) = \cos^{-1}(-7/8), \quad (32)$$

$$\phi_3 = \cos^{-1} \left(-\frac{\hat{\mathbf{n}}_2 \cdot \hat{\mathbf{z}} + (\hat{\mathbf{n}}_3 \cdot \hat{\mathbf{z}})^2}{(\hat{\mathbf{n}}_3 \cdot \hat{\mathbf{x}})^2} \right) = \cos^{-1}(-11/16). \quad (33)$$

These rotation angles then allow us to find the durations of the individual pulses making up $\bar{U}_3(\phi_2)$ and $U_3(\phi_3)$ [together with their inverses $\bar{U}_3(\chi_2)$ and $U_3(\chi_3)$] by solving Eqs. (12) and (14). The resulting full CPHASE pulse sequence for U_5 is given in Sec. V below.

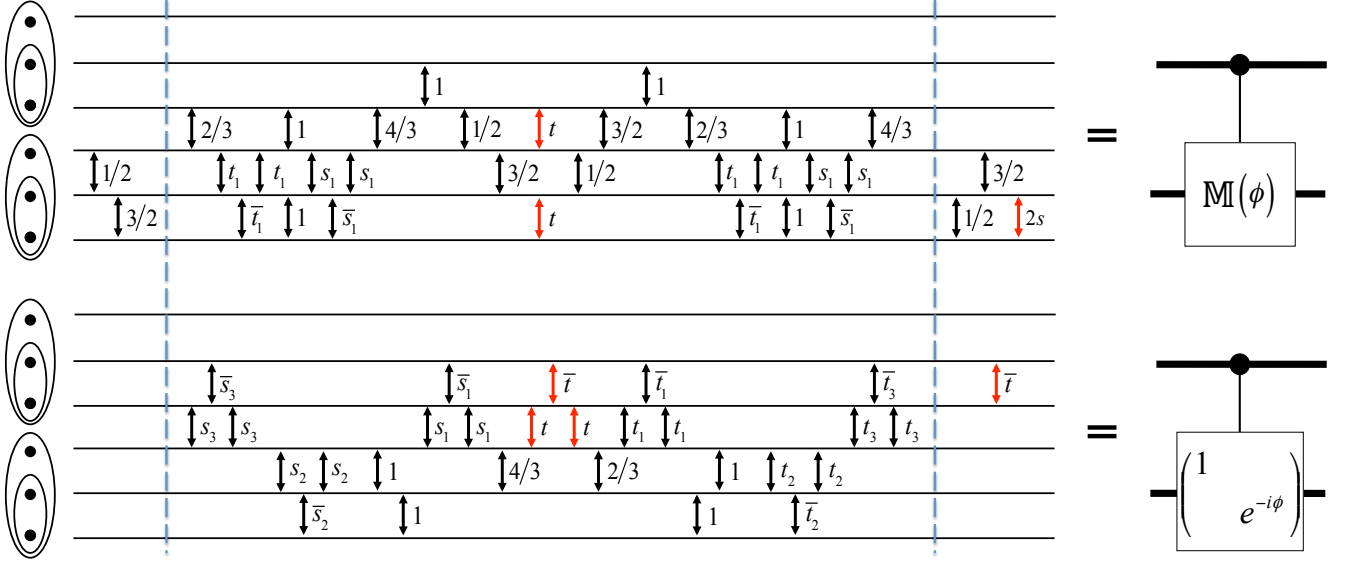


FIG. 8. (Color online) Example two-qubit gates applied to encoded three-spin qubits. Top panel: sequence shown in Fig. 4(c) enacting a controlled-rotation gate (10) with $M = M(\phi)$. Bottom panel: sequence for U_5 shown in Fig. 7 (bottom panel) enacting a CPHASE gate. The pulse durations independent of ϕ , besides those given explicitly in the figure, are: $t_1 = 0.426548$ [34], $t_2 = 0.469699$ and $t_3 = 0.685037$ (see main text); \bar{t}_i for $i = 1, 2, 3$ obtained using Eqs. (12); s_i and \bar{s}_i obtained using the relations $\bar{t}_i + \bar{s}_i = t_i + s_i = 2$ for $i = 1, 2, 3$. The durations of the pulses shown in red depend on the choice of ϕ . For the upper panel, t and s are obtained using $\phi(t)$ as given in Eq. (34); for the lower panel t and \bar{t} are obtained using Eqs. (12) and (14).

V. EXPLICIT PULSE SEQUENCES

Figure 8 shows explicit single-pulse representations of two-qubit gate sequences for the constructions presented above in Secs. III and IV, where single-qubit rotations are carried out by pulses acting before and after the core sequence as indicated by the dashed lines. The gate shown on the top panel of Fig. 8 is locally equivalent to the arbitrary CPHASE gate shown in the bottom panel, both of which are characterized by $\phi \in [0, 2\pi]$. Most pulses appearing in these sequences are independent of ϕ , while those depending on ϕ are shown in red.

The top panel of Fig. 8 shows an explicit two-qubit pulse sequence based on the schematic sequence of T , S and SWAP operations shown in Fig. 4(c). As discussed in Sec. III, this sequence results in an arbitrary controlled rotation gate of the form (10). To obtain this sequence, we substituted for T and S the sequences derived in Appendix B and shown in Figs. 11 and 12, respectively. In addition, simplifications yielding the single-qubit rotations discussed in the appendix have been applied. For the parameterization of the controlled operation (11), i.e., $M(\phi) = e^{i\xi(t)} e^{i\phi(t)\hat{n}(t)\cdot\sigma/2}$, we take from Eq. (B3) that $\xi(t) = -\pi t/2$ and

$$\phi(t) = 2 \arccos((5 \cos(\pi t/2) + 3 \cos(3\pi t/2))/8). \quad (34)$$

Given that $\phi(0) = 0$ and $\phi(t_1) = 2\pi$ with $t_1 = 4 \arctan(\sqrt{2 - \sqrt{3}})$, this pulse sequence can be used to carry out arbitrary controlled-rotation gates using values of $t \in [0, t_1]$.

The lower panel of Fig. 8 shows an explicit pulse sequence based on the sequence for U_5 given in the lower panel of Fig. 7. This sequence is obtained by replacing U_3 , \bar{U}_3 and U_4 by their single-pulse representations given in Fig. 5. To obtain the pulse durations t_2 and t_3 one needs to numerically solve Eqs. (12) and (14) with $\phi = \phi_2$ and ϕ_3 , respectively, as given in Eqs. (32) and (33). As discussed in Sec. IV, the two-qubit gate carried out by this sequence is an arbitrary CPHASE gate of the form (19), where the values of t and \bar{t} depend on the choice of the phase ϕ .

VI. CONCLUSIONS

For spin-based quantum computation in which quantum gates are carried out by exchange-pulse sequences, we have presented two different analytic constructions of entangling two-qubit gates. Up to single-qubit rotations, the resulting sequences can be used to carry out arbitrary CPHASE gates of the form (19), where the phase ϕ can be chosen freely by adjusting the durations of a small number of exchange pulses. Other known two-qubit gate sequences either (i) result in a CNOT gate [6, 29, 30, 36], i.e., a gate locally equivalent to CPHASE with $\phi = \pi$, or (ii) consist of significantly more exchange pulses [34].

When comparing the lengths of different two-qubit gate sequences, the minimum number of pulses depends on the inter-spin connectivity, which is determined by the spin layout assuming only nearest-neighbor pulses. Consider the specific example sequences given in Fig. 8

where the six spins making up two logical qubits are oriented in a linear array. For these two sequences the total number of pulses are 28 (Fig. 8 top) and 25 (Fig. 8 bottom), where, for a basis-independent comparison, we have ignored single-qubit rotations, and continue to do so below. We also consider the layout of maximal connectivity, in which the exchange interaction can be tuned directly between arbitrary spin pairs. As can be deduced using the manipulations introduced in Appendix A, the number of required pulses for our sequences then reduces to the number of pulses different from SWAP; i.e., for each of the above two cases the total number of pulses drops from 28 to 22, and from 25 to 23. Our sequences are thus significantly shorter than those of Ref. [34], which consist of 39 pulses for either layout.

The number of pulses required to carry out the Fong-Wandzura sequence is 18 for spins arranged on a linear array [30], while it is 12 for the case of highest connectivity (also easily established using the manipulations of Appendix A). One way to obtain a CPHASE gate (19) with $\phi \neq \pi$ would be to sandwich a single-qubit operation between two CNOTs; using the optimal Fong-Wandzura sequence this requires at least $2 \times 18 + 1 = 37$ or $2 \times 12 + 1 = 25$ pulses. For either case, our sequences are thus more efficient [39].

To summarize, in Sec. III we generalize the construction of the Fong-Wandzura sequence [30], which can be used to enact a CNOT gate, to a new construction for controlled-rotation gates locally equivalent to arbitrary CPHASE. Starting from the original Fong-Wandzura sequence, we did not simply change the durations of individual pulses but rather altered its fundamental structure. The second two-qubit gate construction, presented in Sec. IV, makes use of smaller pulse sequences whose operations conserve the total spins of certain spin pairs they act on [34]. By doing this, a large subspace of the complete Hilbert space of the six spins encoding two qubits is rendered trivial. The resulting family of two-qubit sequences is, in essence, a streamlined version of that derived in Ref. [34]. In both of these cases, ideas developed in Refs. [33] and [34] were generalized and used to construct entirely new pulse sequences for exchange-only quantum computation.

VII. ACKNOWLEDGMENTS

We thank Joel Pommerening, Veit Langrock and David DiVincenzo for useful discussions.

Appendix A: Rearranging the Fong-Wandzura Pulse Sequence

In this appendix we show explicitly that the Fong-Wandzura pulse sequence, as it was published in Ref. [30], is equivalent to the two-qubit gate sequence that was derived in Ref. [33]. Both of these sequences, which are

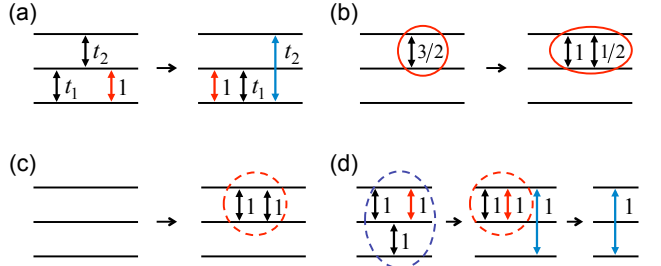


FIG. 9. (Color online) Examples of elementary pulse-sequence manipulations. SWAPS moved past other exchange pulses are shown in red, and pulses whose connectivity is altered by such a move are shown in blue. (a) Moving a SWAP past two pulses of generic durations t_1 and t_2 . (b) Rewriting an inverse $\sqrt{\text{SWAP}}$ as a SWAP followed by a $\sqrt{\text{SWAP}}$ —affected pulses are enclosed by red ovals. (c) Inserting a pair of SWAPS—new pulses are enclosed by the red dashed circle. (d) Simplification of a three-SWAP sequence using (a) followed by the reverse of (c). The three nearest-neighbor SWAPS encircled by a blue dashed oval are thus equivalent to a single next-nearest neighbor SWAP. Note that all reversed diagrams are true as well.

shown in Fig. 2, consist only of nearest-neighbor exchange pulses, assuming the spins that these sequences act on are placed on a linear array. These sequences can be transformed into one another by carrying out a series of elementary manipulations in which pairs of SWAPS, i.e., exchange pulses of duration 1, are inserted into a pulse sequence, or single SWAPS are moved past, or combined with, other pulses.

Figure 9 exemplifies a number of such manipulations by means of short pulse sequences acted on three spin- $\frac{1}{2}$ particles. Figure 9(a) shows two equivalent sequences. The one on the left-hand side (LHS) of the figure consists of three nearest-neighbor pulses, beginning with a pulse of duration t_1 acting on the lower two spins, followed by a pulse of duration t_2 acting on the upper two spins, and ending with a SWAP acting on the lower two spins. The equivalent sequence on the right-hand side (RHS) of the same figure consists of a SWAP followed by a t_1 -pulse, both of which act on the lower two spins, and ends with a next-nearest neighbor t_2 -pulse acting on the uppermost and lowermost spins. The equivalence of these sequences becomes evident upon replacing the SWAPS with spin permutations. One way to manipulate pulse sequences is thus to move SWAPS past other pulses while taking note if after such a move these other pulses act on different spins than before. As also shown in Fig. 9(a), in this appendix we adopt the convention that SWAPS moved past other pulses are shown in red, and exchange pulses altered by such a move are shown in blue.

Another way of manipulating a pulse sequence, which is exemplified in Fig. 9(b), is that of replacing an inverse $\sqrt{\text{SWAP}}$ (pulse of duration 3/2) with a SWAP followed by a $\sqrt{\text{SWAP}}$ (pulse of duration 1/2). This is allowed because an exchange pulse acting on a pair spins of duration t_1+t_2

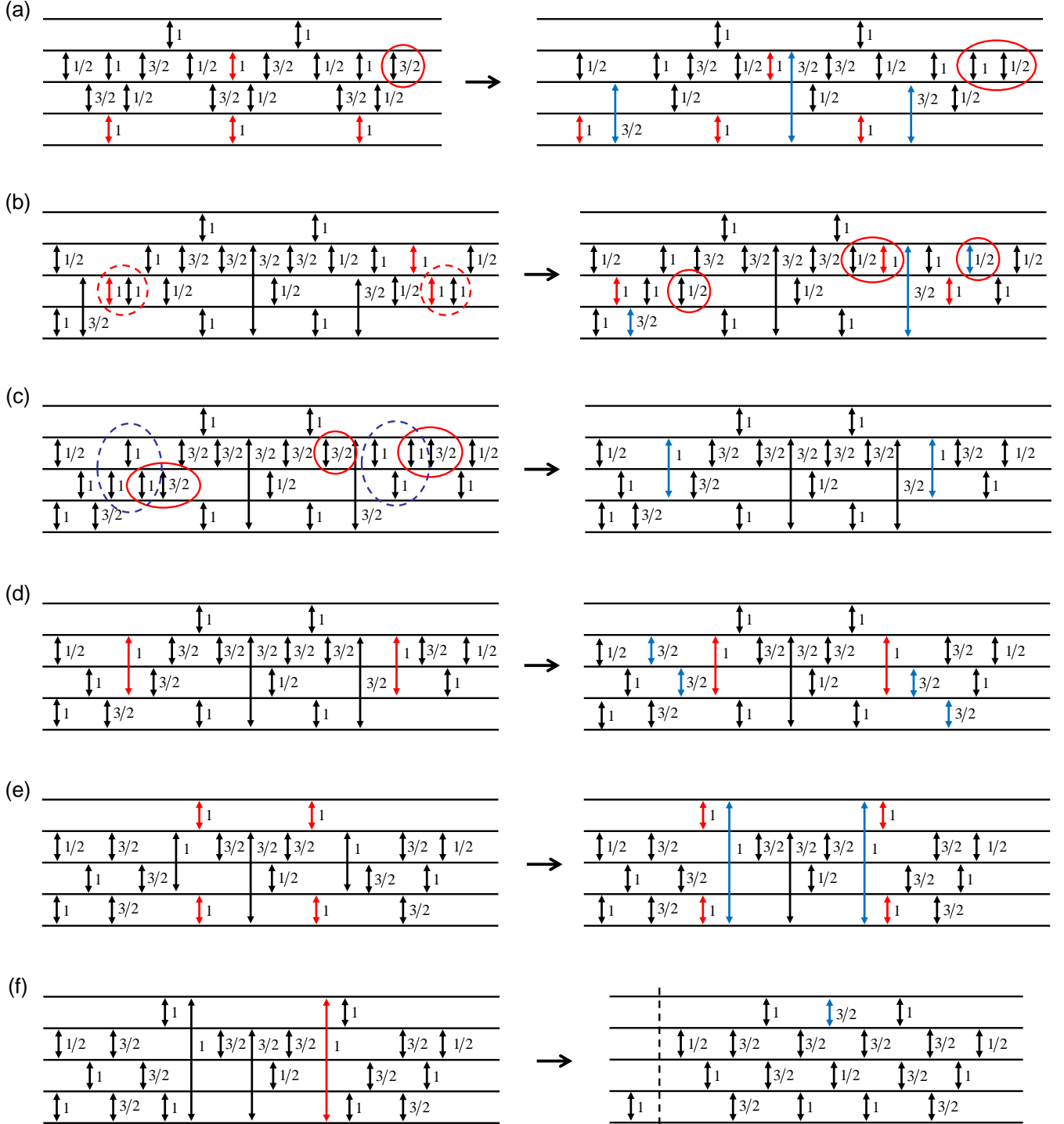


FIG. 10. (Color online) Series of elementary manipulations that turns the core Fong-Wandzura sequence that was analytically derived in Ref. [33] into its equivalent form originally published in Ref. [30], thus proving the statement made in Fig. 2. To the left of the dashed line in (f) there is an additional SWAP, which can be absorbed into a single-qubit rotation.

is equivalent to two consecutive pulses acting on the same pair of spins with durations t_1 and t_2 . As a last example of an elementary manipulation, consider Fig. 9(c). As shown in the figure, we can insert (remove) a pair of

SWAPs into (from) a pulse sequence because the effect of two consecutive SWAPs is the same as applying the identity. Note that when the number of pulses changes due to a manipulation step [as in Figs. 9(b) and (c)] we

enclose the involved pulses inside an oval.

As an example of using some of the above manipulations, consider the three pulse sequences shown in Fig. 9(d). The leftmost sequence consists of three nearest-neighbor SWAPS (enclosed by a blue oval) with the first and the last acting on the upper two spins, and the central SWAP acting on the lower two spins. In the first step we move the rightmost SWAP, shown in red, past the central pulse, yielding the second sequence in Fig. 9(d). Due to this move, the now rightmost pulse, shown in blue, is a next-nearest neighbor SWAP that acts on the uppermost spin and the lowermost spin. Finally, since after this move the leftmost SWAP and the red SWAP are located directly next to each other we are allowed to remove this pair of pulses from the sequence.

With these basic manipulation steps in hand we are now ready to convert the two-qubit gate sequence shown on the LHS of Fig. 2, which has been derived in Ref. [33], into the originally published Fong-Wandzura sequence [30] shown on the RHS of the same figure. Figure 10 contains the transformation that shows this equivalence, where we apply the two-qubit gate sequences on five of the six spins that are used to encode two qubits.

Beginning with the sequence shown on the LHS of Fig. 2, in Fig. 10(a) we move the four SWAPS shown in red to the left; their original and final positions are given on the LHS and RHS of the figure, respectively. Similar to the example of Fig. 9(a), the pulses that are shown in blue have been altered by these moves. Furthermore, similar to Fig. 9(b), the rightmost inverse $\sqrt{\text{SWAP}}$ in the sequence on the LHS of Fig. 10(a) has been replaced with a SWAP and a $\sqrt{\text{SWAP}}$ (as indicated by the red ovals). The next step begins with the sequence shown on the LHS of Fig. 10(b), which is the result of taking the previous sequence [i.e. that shown on the RHS of Fig. 10(a)] and, similar to the example in Fig. 9(c), inserting two pairs of SWAPS, which are enclosed in dashed circles. The three red SWAPS on the LHS of Fig. 10(b) are then moved towards the left with their final positions given in the sequence on the RHS of the figure.

When turning to the sequence on the LHS of Fig. 10(c), the $\sqrt{\text{SWAP}}$ and its neighboring SWAP enclosed by an oval in the sequence on the RHS of Fig. 10(b) are replaced with an inverse $\sqrt{\text{SWAP}}$. Furthermore, the two individually circled $\sqrt{\text{SWAP}}$ s on the RHS of Fig. 10(b) have each been replaced by a pair of pulses in Fig. 10(c). In the transition to the RHS of this figure, we use the identity shown in Fig. 9(d) to replace each of the three SWAPS encircled by a blue dashed oval by a single next-nearest neighbor SWAP.

The remaining task is to remove these two next-nearest neighbor SWAPS by placing them directly next to each other. For clarity, this is done in several steps shown in Figs. 10(d)-(f). First, in (d) we move both of these red SWAPS towards the center of the sequence where, as usual, pulses that have been altered are shown in blue. Rather than moving the same pulses further towards each other, in (e) we take the four red nearest-neighbor SWAPS and

move each of them one step towards the outside of the sequence, thus altering the next-nearest neighbor SWAPS. Finally, in (f) we take the SWAP shown in red and move it towards the left where it is combined with its equivalent SWAP, and thus removed. Note that in this last manipulation only a single exchange pulse is altered.

In the resulting sequence of nearest-neighbor pulses, which is shown on the RHS of Fig. 10(f), we use a dashed line to separate out a SWAP, which can be absorbed by a single-qubit rotation. This final sequence is thus locally equivalent to the that given on the RHS of Fig. 2.

Appendix B: Explicit Pulse Sequences for the T and S Operations

In Sec. III, a set of two-qubit gate sequences was constructed using the operations T and S defined in Eqs. (8) and (9), respectively. In this appendix we design example pulse sequences that can be used to carry out these operations, and which are the ones used for the explicit sequences presented in Sec. V.

As shown in Fig. 4(c), the operations T and S are applied to four spin- $\frac{1}{2}$ particles, three of which, initialized with total spin $\frac{1}{2}$, are represented by the symbol \star . In order to design explicit pulse sequences, we first abandon the notation \star by effectively reversing Eq. (3), so that the Hilbert space of \bullet and \star is now spanned by four states

$$(\bullet\star)_d \rightarrow (\bullet(\bullet(\bullet\bullet)_b)_{c=1/2})_d \quad (B1)$$

with $b = 0$ or 1 for both $d = 0$ and 1 . Since an exchange pulse acting on the two leftmost spins on the RHS of Eq. (B1) will not conserve the total spin of the rightmost three qubits, denoted by c , we need to consider a five-dimensional Hilbert space spanned by the states $(\bullet(\bullet(\bullet\bullet)_b)_c)_d$ with $bc = 0\frac{1}{2}$ and $1\frac{1}{2}$ for $d = 0$ and $bc = 0\frac{1}{2}$, $1\frac{1}{2}$ and $1\frac{3}{2}$ for $d = 1$. Recall, however, that in Sec. III we imposed the condition that applying the full sequence of T or S conserve this quantum number c .

Figure 11 contains the essence of our derivation of a pulse sequence that realizes T . Figure 11(a) shows the sequence used for T as it is applied to four spins labeled 1 through 4, that is,

$$T = U_{34}(2s)V^{-1}U_{12}(t)U_{34}(t)V. \quad (B2)$$

Here U_{ij} , as introduced in Eq. (1), represents an exchange pulse acting on individual spins i and j , and V represents a pulse sequence yet to be determined. The sequence (B2) can then be understood as a similarity transformation of the two central t -pulses $U_{12}(t)U_{34}(t)$ carried out by V , which is followed by the operation $U_{34}(2s)$.

To find the matrix representation of this T operation, first note that using Eq. (1) it is straightforward to find the matrix associated with the two central pulses of duration t in the basis $((\bullet\bullet)_b'(\bullet\bullet)_b)_d$. The resulting matrix, for simplicity given up to an overall phase factor, is shown

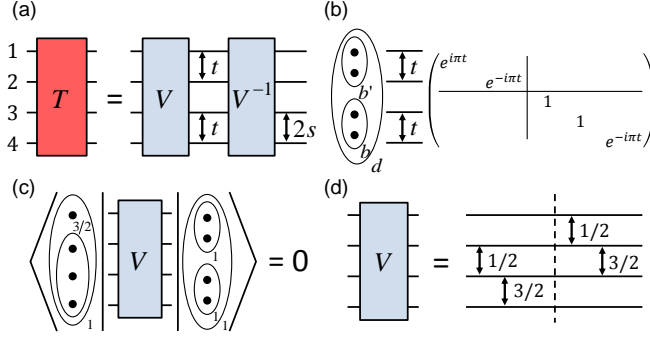


FIG. 11. Construction of a pulse sequence for the T operation. (a) Schematic pulse sequence for T applied to four spins labeled 1 through 4, where $s = 2 - t$. (b) Matrix representation of the operation due to the central t -pulses in the indicated basis with state ordering $bb'd = \{000, 110|011, 101, 111\}$. (c) Crucial constraint placed on the operation V . (d) Explicit pulse sequence for V . The dashed line separates the optimal V -sequence satisfying (c), $V_0 = U_{23}(\frac{3}{2})U_{12}(\frac{1}{2})$, from the additional pulses used to satisfy the condition imposed by Eq. (8).

in Fig. 11(b). We now examine the effect of the remaining operations in Eq. (B2) on this central operation in each of the total-spin $d = 0$ and 1 sectors.

First considering the total-spin $d = 1$ subspace, we place the constraint shown in Fig. 11(c) on the operation V . This constraint implies that after applying V to the state $(\bullet(\bullet\bullet)_{c=3/2})_1$, the outcome has no overlap with the state $((\bullet\bullet)_{b'=1}(\bullet\bullet)_{b=1})_1$, and accordingly lies completely in the $((\bullet\bullet)_{b'}(\bullet\bullet)_b)_1$ sector with $bb' = 01$ and 10. Note that in this subspace the operation $U_{12}(t)U_{34}(t)$ is proportional to the identity [cf. Fig. 11(b)] and thus leaves the state unchanged, so that the operation V^{-1} maps this state back to the original state, $(\bullet(\bullet\bullet)_{3/2})_1$. Since the operation $V^{-1}U_{12}(t)U_{34}(t)V$ thus maps this $c = \frac{3}{2}$ state back onto itself, and further the final pulse in Eq. (B2), $U_{34}(2s)$, merely applies a phase factor to this state, it follows that the T operation also maps the two-dimensional $c = \frac{1}{2}$ sector onto itself.

In the derivation of the Fong-Wandzura sequence in Ref. [33] an argument similar to that just made was used to find a pulse sequence for the R -operation of Fig. 3(a). In doing this, the optimal sequence for such a V operation satisfying the constraint in Fig. 11(c) was analytically determined to be $V_0 = U_{23}(\frac{3}{2})U_{12}(\frac{1}{2})$.

Figure 11(d) shows the V sequence used in our construction, which is $V = U_{23}(\frac{3}{2})U_{12}(\frac{1}{2})U_{34}(\frac{3}{2})U_{23}(\frac{1}{2}) = V_0U_{34}(\frac{3}{2})U_{23}(\frac{1}{2})$. We use this longer sequence for V in order to obtain the matrix representation of T given in Eq. (8) [40]. Given that V_0 satisfies the constraint in Fig. 11(c), it is straightforward to see that our longer V sequence also satisfies that constraint. This is most easily seen by replacing the V sequence in Fig. 11(c) with its single-pulse representation shown in Fig. 11(d). The two pulses to the left of the dashed line can then be absorbed by the state $(\bullet(\bullet\bullet)_{3/2})_1$ at the cost of applying simple

overall phase factors (since any pair of spins within the oval with total spin $\frac{3}{2}$ has total spin 1), which do not alter the fact that this overlap vanishes.

The matrix representation of T in the $d = 1$ sector is determined in Appendix D 2. This is done by finding the matrix of each pulse in an appropriate eigenbasis using Eq. (1), and then carrying out the required basis changes to the b -basis (B1) for $d = 1$; these basis changes are summarized in Appendix D 1. In this b -basis with the state ordering $b = \{0, 1\}$ we take from Eq. (D36) that

$$\mathbb{M} = e^{-i\pi t/2} e^{i\pi(2-t)\hat{\mathbf{z}} \cdot \boldsymbol{\sigma}} e^{-i\pi t \hat{\mathbf{n}}_1 \cdot \boldsymbol{\sigma}/2}, \quad (B3)$$

where $\hat{\mathbf{n}}_1 = (\sqrt{3}/4, -\sqrt{3}/2, 1/4)$.

To determine the unitary operation of T on the $d = 0$ Hilbert space, note that here the two four-spin states in the basis shown in Fig. 11(b) are given by $((\bullet\bullet)_{b'}(\bullet\bullet)_b)_0$ with $bb' = 00$ or 11, and thus $b' = b$. A direct result of this is that

$$U_{12}(t) = U_{34}(t), \quad (d = 0), \quad (B4)$$

so that the two central pulses within V , $U_{12}(\frac{1}{2})$ and $U_{34}(\frac{3}{2})$, cancel one another. Since the outer two pulses are inverses of each other as well, we conclude that $V = \mathbb{1}$ ($d = 0$). Equation (B4) further implies that the remaining three pulses within the T sequence [shown explicitly in Fig. 11(a)] cancel, so that $T = \mathbb{1}$ for $d = 0$ as required by Eq. (8).

Before we turn our attention to finding a sequence for the S operation, we make a comment on the T sequence of Fig. 11(a), which, upon unpacking V using Fig. 11(d), can be written as

$$\begin{aligned} T = & U_{34}(2s)U_{23}(\frac{3}{2})U_{34}(\frac{1}{2}) \times \\ & [U_{12}(\frac{3}{2})U_{23}(\frac{1}{2})U_{12}(t)U_{34}(t)U_{12}(\frac{1}{2})U_{23}(\frac{3}{2})] \times \\ & U_{34}(\frac{3}{2})U_{23}(\frac{1}{2}). \end{aligned} \quad (B5)$$

Recall that T is the central operation in the two-qubit gate sequence shown in Fig. 4(c). As shown in the top panel of Fig. 8, all five pulses outside square brackets in Eq. (B5), i.e., $U_{34}(2s)U_{23}(\frac{3}{2})U_{34}(\frac{1}{2})$ and $U_{34}(\frac{3}{2})U_{23}(\frac{1}{2})$, have been pulled out of the two-qubit sequence (thus playing the role of single-qubit rotations). The reason we are allowed to do this is that these five pulses commute with S , since they exclusively act on the internal Hilbert space of the lower qubit with state label b , and the surrounding S operations act on this lower-qubit space as the identity [cf. Eq. (9)].

Figure 12(a) shows a four-spin pulse sequence that realizes the S operation, which, again labeling the spins 1 through 4, can be written as

$$S = W^{-1}U_{12}(1)U_{34}(1)W. \quad (B6)$$

Similar to the schematic sequence V in the sequence (B2) for the T operation, here S is formulated using an operation W whose pulse sequence is yet to be determined. Note that W carries out a similarity transformation on the central two SWAPS.

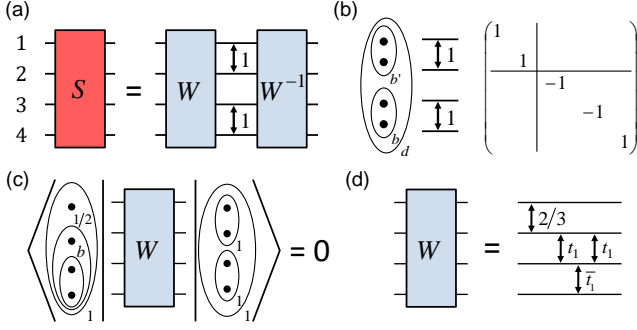


FIG. 12. Construction of a pulse sequence for the elevated SWAP operation S . (a) Schematic sequence for S applied to four spins labeled 1 through 4. (b) Matrix representation of the operation due to the central SWAP pulses in the indicated basis with state ordering $bb'd = \{000, 110|011, 101, 111\}$. (c) Constraints placed on W for both $b = 0$ and 1 . (d) Explicit sequence for W with pulse durations t_1 and \bar{t}_1 given in Fig. 8.

We evaluate the S -sequence by first noting the matrix representation of the central SWAPS in Fig. 12(b) in the indicated bb' -basis $((\bullet\bullet)_{b'}(\bullet\bullet)_b)_d$, which is obtained easily using Eq. (1). Comparing this matrix with that in Eq. (9) [given in the basis (B1)], we find agreement not only for $d = 0$, but also for $d = 1$ upon focusing on the $bb' = 01, 10$ matrix sector in Fig. 12(b). Since these matrices are given in different bases, the operation W in Eq. (B6) needs to map the b -basis (B1) to the $bb' = 01, 10$ sector of the bb' basis for both $d = 0$ and 1 .

Note that since for $d = 0$ the central SWAPS in Eq. (B6) carry out the identity operation [see Fig. 12(b)], here this change of bases is trivially accomplished by any sequence W . In case of $d = 1$, however, we need to ensure that applying W to the states $(\bullet(\bullet(\bullet\bullet)_b)_{1/2})_1$ with $b = 0$ or 1 , which span the b -basis (B1) for $d = 1$, yield states orthogonal to $((\bullet\bullet)_1(\bullet\bullet)_1)_1$. As shown in Fig. 12(c), we place this very constraint on W . Note that since the operation due to the central SWAPS in Eq. (B6) is proportional to the identity in the $bb' = 10, 01$ sector [again, see Fig. 12(b)], the precise form of the basis change carried out by W is irrelevant [i.e., the condition shown in Fig. 12(c) is sufficient]. The pulse sequence for W shown in Fig. 12(d) was analytically designed in Ref. [34] to carry out such a basis change.

Appendix C: Computation of Pseudospin Rotations

In Sec. IV, two-qubit gate sequences are constructed using the operations U_3 , \bar{U}_3 and U_4 . The explicit sequences for these operations are given in Fig. 5 where U_3 and \bar{U}_3 are applied to three spin- $\frac{1}{2}$ particles while U_4 is applied to four spin- $\frac{1}{2}$ particles. In Fig. 6 these operations act on the five spins

$$((\bullet\bullet)_a(\bullet(\bullet\bullet)_b)_c)_f, \quad (C1)$$

where $a, b = 0$ or 1 and $c, f = \frac{1}{2}$ or $\frac{3}{2}$.

As described in Sec. IV, we effectively reduce the Hilbert space dimensionality by setting $a, b \rightarrow 1$. Upon introducing an effective spin-1 particle, $\Delta = (\bullet\bullet)_1$, as in Eqs. (20) and (21), this Hilbert space is spanned by the states

$$(\Delta(\bullet\Delta)_c)_f \quad (C2)$$

with $cf = \frac{1}{2}\frac{1}{2}, \frac{3}{2}\frac{1}{2}, \frac{1}{2}\frac{3}{2}$ and $\frac{3}{2}\frac{3}{2}$, and so breaks into two two-dimensional sectors with total spin $f = \frac{1}{2}$ and $\frac{3}{2}$.

In what follows, we discuss in C1 why we are allowed to simplify the Hilbert space basis (C1) to (C2), and what needs to be taken into account when doing so. C2 then contains derivations of the matrix representations of the operations U_3 , \bar{U}_3 and U_4 .

1. Effective Hilbert Space

As discussed in Sec. IV, the operations U_3 , \bar{U}_3 , and U_4 as arranged in Fig. 6 conserve the quantum numbers a and b . It is thus natural to divide the Hilbert space into four different sectors with $ab = 00, 01, 10$ and 11 , which can be considered independently. We now explain why each of these three operations acts trivially on the states (C1) with $a = 0$ or $b = 0$, a fact that allows us to focus on the effective Hilbert space spanned by the states (C2).

The operation U_4 acting on the spins (C1) as shown in Fig. 6(a) is accompanied on either side by a generalized SWAP operation. These operations exchange the spin pair $(\bullet\bullet)_b$ with the single spin \bullet , which are enclosed by the oval with total spin c , that is,

$$(\bullet(\bullet\bullet)_b)_c \longleftrightarrow ((\bullet\bullet)_b\bullet)_c. \quad (C3)$$

Because of this, the sequence of U_4 can equivalently be regarded as directly acting on the leftmost four spins in the basis

$$((\bullet\bullet)_a((\bullet\bullet)_b\bullet)_c)_f. \quad (C4)$$

If $a = 0$ or $b = 0$, respectively, these five spins are in the states

$$((\bullet\bullet)_0((\bullet\bullet)_b\bullet)_c)_f = (((\bullet\bullet)_0(\bullet\bullet)_b)\bullet)_f \quad (C5)$$

or

$$((\bullet\bullet)_a((\bullet\bullet)_0\bullet)_c)_f = (((\bullet\bullet)_a(\bullet\bullet)_0)\bullet)_f, \quad (C6)$$

where $c, f = \frac{1}{2}$ or $\frac{3}{2}$. Note that for both of these states as expressed on the RHS of these equations, the leftmost four spins are given in the natural basis shown on the far left in Fig. 5(c), in which we introduced the operation U_4 . It then follows from Eq. (16) that the action of U_4 on the state (C1) with $a = 0$ [taking into account the surrounding SWAPS (C3)] is that of applying a simple phase factor independent of the value of b . Similarly, from Eq. (17) we find that the action of U_4 on all $b = 0$ states (C1) is that of the identity.

The operation \bar{U}_3 shown in Fig. 6(b) acts on the lowermost three spins, and is thus independent of a . If $b = 0$, the spins (C1) are in the states

$$((\bullet\bullet)_a(\bullet(\bullet\bullet)_0)_{1/2})_f, \quad (C7)$$

where $a = 0$ or 1 and $f = \frac{1}{2}$ or $\frac{3}{2}$. The action of \bar{U}_3 on the rightmost three spins is given by Eq. (15) for the case of $a' = 0$, and is that of applying an overall phase factor to all $b = 0$ states. Similarly, the operation U_3 shown in Fig. 6(c) acts on the uppermost three spins and is therefore independent of b . Since for $a = 0$ the spins (C1) are in the states

$$((\bullet\bullet)_0(\bullet(\bullet\bullet)_b)_c)_{f=c} = (((\bullet\bullet)_0\bullet)_{1/2}(\bullet\bullet)_b)_{f=c}, \quad (C8)$$

where $b = 0$ or 1 and $c = \frac{1}{2}$ or $\frac{3}{2}$, the action of U_3 on the leftmost three spins is given in Eq. (13) for the case of $a = 0$, and is that of applying an overall phase factor to all $a = 0$ states.

In summary, when applying any one of the operations shown in Fig. 6 to the states (C1) with $a = 0$ or $b = 0$, the result is either the identity operation or the multiplication by a phase factor that depends on only one of the qubit states. These phases are simple to keep track of, and can be canceled by appropriate single-qubit rotations before or after the two-qubit gate sequence. We can thus ignore the cases of $a = 0$ or $b = 0$, and work in the effective Hilbert space spanned by the states (C2).

2. Matrix Representations in Pseudospin Space

To describe the action of the operations U_3 , \bar{U}_3 , and U_4 in the basis (C2), we introduce a corresponding pseudospin for both the $f = \frac{1}{2}$ and $\frac{3}{2}$ sectors. Each pseudospin space is spanned by the states

$$\uparrow_f = (\blacktriangle(\bullet\blacktriangle)_{c=1/2})_f, \quad \downarrow_f = (\blacktriangle(\bullet\blacktriangle)_{c=3/2})_f. \quad (C9)$$

For simplicity, below we refer to these spaces as \uparrow_f .

The operation U_4 is shown in Fig. 6(a). Its matrix representation is given most easily in its natural basis,

$$((\blacktriangle\blacktriangle)_d\bullet)_f, \quad (C10)$$

which will be related to the pseudospins \uparrow_f further below. If $f = \frac{1}{2}$, we find from Eq. (17) for the case of $b = 1$ with basis ordering $d = \{0, 1\}$,

$$U_{4,d}^{f=1/2}(\phi) = \text{diag}(1, e^{-i\phi}) = e^{-i\phi/2} e^{i\phi\hat{\mathbf{z}}\cdot\boldsymbol{\sigma}/2}. \quad (C11)$$

Here the subscript in the notation $U_{4,d}^{f=1/2}$ indicates the basis. If $f = \frac{3}{2}$, we similarly find with $d = \{1, 2\}$,

$$U_{4,d}^{f=3/2}(\phi) = \text{diag}(e^{-i\phi}, e^{-i\phi}) = e^{-i\phi}\mathbb{1}. \quad (C12)$$

We perform the basis change from the d -basis (C10) to the pseudospin \uparrow_f basis given in Eq. (24) in two

steps. First, we introduce another two pseudospin spaces spanned by the states

$$\uparrow'_f = (\blacktriangle(\blacktriangle\bullet)_{c=1/2})_f, \quad \downarrow'_f = (\blacktriangle(\blacktriangle\bullet)_{c=3/2})_f \quad (C13)$$

with $f = \frac{1}{2}$ or $\frac{3}{2}$, which will be referred to below as \uparrow'_f , and give the action of U_4 on this pseudospin. Note that the \uparrow'_f basis is related to the d -basis (C10) by a basis change that consists of shifting ovals. In the second step, we use the generalized SWAP operation that exchanges the particles $\blacktriangle = (\bullet\bullet)_1$ and \bullet introduced above [as described in Eq. (C3) for $b = 1$], to relate the pseudospin bases \uparrow'_f and \uparrow_f to one another. This pseudospin transformation is realized by the indicated particle exchanges surrounding U_4 in Fig. 6(a). The action of this generalized SWAP operation, as discussed in Appendix D 3, is to produce a relative phase factor of -1 between the states with $c = \frac{1}{2}$ and $\frac{3}{2}$. This action can thus be interpreted as a π rotation about the z axis when relating \uparrow'_f to \uparrow_f , i.e.,

$$U_{4,\uparrow_f} = e^{i\pi\hat{\mathbf{z}}\cdot\boldsymbol{\sigma}/2} U_{4,\uparrow'_f} e^{i\pi\hat{\mathbf{z}}\cdot\boldsymbol{\sigma}/2} \quad (C14)$$

for both the $f = \frac{1}{2}$ and $\frac{3}{2}$ sectors.

Since the action of U_4 for $f = \frac{3}{2}$ is proportional to the identity [cf. Eq. (C12)], here the two-step basis change has no effect,

$$U_{4,\uparrow_{3/2}}(\phi) = U_{4,d}^{f=3/2}(\phi) = e^{-i\phi}\mathbb{1}. \quad (C15)$$

Changing bases in the $f = \frac{1}{2}$ sector is less trivial. The first step, in which we change from the d -basis (C10) to the pseudospin $\uparrow'_{1/2}$ basis, has been carried out explicitly in Ref. [34] [see Eqs. (17)-(21) therein] with the result that U_4 performs a pseudospin rotation

$$U_{4,\uparrow'_{1/2}}(\phi) = e^{-i\phi/2} e^{i\phi\hat{\mathbf{n}}'_2\cdot\boldsymbol{\sigma}/2} \quad (C16)$$

about an axis $\hat{\mathbf{n}}'_2 = (-2\sqrt{2}/3, 0, -1/3)$ through angle ϕ . The second step given in Eq. (C14), which is the transformation from \uparrow'_f to \uparrow_f , has the effect of rotating the vector $\hat{\mathbf{n}}'_2$ about the z axis through angle π onto the vector $\hat{\mathbf{n}}_2 = (2\sqrt{2}/3, 0, -1/3)$,

$$\begin{aligned} U_{4,\uparrow_{1/2}}(\phi) &= e^{i\pi\sigma_z/2} U_{4,\uparrow'_{1/2}}(\phi) e^{i\pi\sigma_z/2} \\ &= e^{-i\phi/2} e^{i\pi\sigma_z/2} e^{i\phi\hat{\mathbf{n}}'_2\cdot\boldsymbol{\sigma}/2} e^{i\pi\sigma_z/2} \\ &= e^{-i\phi/2} e^{i\phi\hat{\mathbf{n}}_2\cdot\boldsymbol{\sigma}/2}. \end{aligned} \quad (C17)$$

This $f = \frac{1}{2}$ pseudospin rotation is indicated in Fig. 6(a).

Next we determine the action of the two different U_3 operations shown in Figs. 6(b) and (c) on the pseudospin space \uparrow_f given in Eq. (C9). To do this, we write both matrix representations in the basis (C2). The operation \bar{U}_3 shown in Fig. 6(b) conserves the quantum number c , so we can take its matrix in the basis $c = \{\frac{1}{2}, \frac{3}{2}\}$ directly from Eq. (15) for $a' = 1$,

$$\bar{U}_{3,c}(\phi) = \text{diag}(1, e^{-i\phi}) = e^{-i\phi/2} e^{i\phi\hat{\mathbf{z}}\cdot\boldsymbol{\sigma}/2}, \quad (C18)$$

which corresponds to a z -axis rotation in each pseudospin space \uparrow_f .

The matrix representation of the U_3 operation in Fig. 6(c) can be found most easily in the basis $((\Delta\bullet)_{c'}\Delta)_{1/2}$. For basis ordering $c' = \{\frac{1}{2}, \frac{3}{2}\}$, we find from Eq. (13) for the case of $a = 1$ that this matrix is the same as that given in Eq. (C18). Carrying out the basis change given below in Appendix D [see Eqs. (D7)-(D9)], in particular the definition of the matrix $F_3 = \hat{\mathbf{f}}_3 \cdot \boldsymbol{\sigma}$ with $\hat{\mathbf{f}}_3 = (2\sqrt{2}/\sqrt{3}, 0, -1/3)$, we find the matrix of U_3 in the basis (C2) with $c = \{\frac{1}{2}, \frac{3}{2}\}$,

$$U_{3,c}(\phi) = F_3 \text{diag}(1, e^{-i\phi}) F_3 = e^{-i\phi/2} e^{i\phi \hat{\mathbf{n}}_3 \cdot \boldsymbol{\sigma}/2} \quad (\text{C19})$$

where $\hat{\mathbf{n}}_3 = 2\hat{\mathbf{f}}_3(\hat{\mathbf{f}}_3 \cdot \hat{\mathbf{z}}) - \hat{\mathbf{z}} = (-4\sqrt{2}/9, 0, -7/9)$. The operation \overline{U}_3 is thus a rotation about $\hat{\mathbf{n}}_3$ in each pseudospin space \uparrow_f .

Appendix D: Basis Changes and Qubit Rotations

We now present further detailed derivations of matrix representations of unitary operations due to pulse sequences introduced above. All required basis changes are presented in D 1. In D 2 we consider the T sequence introduced in Sec. III for the case of the explicit pulse sequence given in Appendix B. Finally, D 3 contains a derivation of the action of the generalized SWAP introduced in Sec. IV.

1. Basis Changes

We begin by describing a number of required basis changes. First, consider three spin- $\frac{1}{2}$ particles with total spin $\frac{1}{2}$ in the standard qubit basis $(\bullet(\bullet\bullet)_a)_{1/2}$ with $a = 0$ or 1, as also shown in Fig. 1(a). Another basis for this three-spin Hilbert space is $((\bullet\bullet)_a' \bullet)_{1/2}$ with $a' = 0$ or 1, which can be related to the former basis via

$$((\bullet\bullet)_a' \bullet)_{1/2} = \sum_{a=0,1} F_{1,a'a} (\bullet(\bullet\bullet)_a)_{1/2} \quad (\text{D1})$$

with the recoupling coefficients

$$F_{1,a'a} = \langle (\bullet(\bullet\bullet)_a)_{1/2} | ((\bullet\bullet)_a' \bullet)_{1/2} \rangle. \quad (\text{D2})$$

To fix the phases of these coefficients we must at this point adopt a phase convention for our total-spin basis states. Here and in all that follows we use the standard Condon-Shortley convention [41]. For this choice, the recoupling coefficients form the transformation matrix

$$F_1 = \begin{pmatrix} -1/2 & \sqrt{3}/2 \\ \sqrt{3}/2 & 1/2 \end{pmatrix} = \hat{\mathbf{f}}_1 \cdot \boldsymbol{\sigma} \quad (\text{D3})$$

with $\hat{\mathbf{f}}_1 = (\sqrt{3}/2, 0, -1/2)$ which maps the basis $a = \{0, 1\}$ to the basis $a' = \{0, 1\}$. Note that $F_1^\dagger = F_1$.

For the next basis change, consider four spin- $\frac{1}{2}$ particles with total spin 1 in the basis $((\bullet\bullet)_b' (\bullet\bullet)_b)_1$, which is also shown in Fig. 11(b). If we let $b \rightarrow 1$ and introduce an effective spin-1 particle $\Delta = (\bullet\bullet)_1$ as in Eq. (20), we obtain a two-dimensional, effective Hilbert space of two spin- $\frac{1}{2}$ particles and one spin-1 particle with total spin 1. We can now relate the basis $((\bullet\bullet)_b' \Delta)_1$ with $b' = 0$ and 1 to an alternate basis $(\bullet(\bullet\Delta)_c)_1$ with $c = \frac{1}{2}$ or $\frac{3}{2}$,

$$(\bullet(\bullet\Delta)_c)_1 = \sum_{b'=0,1} F_{2,cb'} ((\bullet\bullet)_b' \Delta)_1, \quad (\text{D4})$$

where the recoupling coefficients are given by

$$F_{2,cb'} = \langle ((\bullet\bullet)_b' \Delta)_1/2 | (\bullet(\bullet\Delta)_c)_1/2 \rangle. \quad (\text{D5})$$

The transformation matrix

$$F_2 = \begin{pmatrix} -1/\sqrt{3} & \sqrt{2/3} \\ \sqrt{2/3} & 1/\sqrt{3} \end{pmatrix} = \hat{\mathbf{f}}_2 \cdot \boldsymbol{\sigma}, \quad (\text{D6})$$

where $\hat{\mathbf{f}}_2 = (\sqrt{2/3}, 0, -1/\sqrt{3})$ and $F_2^\dagger = F_2$, then maps the basis $c = \{\frac{1}{2}, \frac{3}{2}\}$ to $b' = \{0, 1\}$.

Finally, we consider the basis change for the Hilbert space spanned by one spin- $\frac{1}{2}$ and two spin-1 particles. We begin from the basis $(\Delta(\bullet\Delta)_c)_{f=1/2}$ with $c = \frac{1}{2}$ or $\frac{3}{2}$, which is shown in Fig. 6. Now consider the alternate basis $((\Delta\bullet)_c' \Delta)_{f=1/2}$ with $c' = \frac{1}{2}$ and $\frac{3}{2}$, which can be expressed in terms of the c -basis states by

$$((\Delta\bullet)_c' \Delta)_{1/2} = \sum_{c=\frac{1}{2},\frac{3}{2}} F_{3,c'c} (\Delta(\bullet\Delta)_c)_{1/2}, \quad (\text{D7})$$

where

$$F_{3,c'c} = \langle (\Delta(\bullet\Delta)_c)_{1/2} | ((\Delta\bullet)_c' \Delta)_{1/2} \rangle. \quad (\text{D8})$$

The transformation matrix

$$F_3 = \begin{pmatrix} -1/3 & 2\sqrt{2}/3 \\ 2\sqrt{2}/3 & 1/3 \end{pmatrix} = \hat{\mathbf{f}}_3 \cdot \boldsymbol{\sigma}, \quad (\text{D9})$$

where $\hat{\mathbf{f}}_3 = (2\sqrt{2}/3, 0, -1/3)$ and $F_3^\dagger = F_3$, then maps the basis $c = \{\frac{1}{2}, \frac{3}{2}\}$ to $c' = \{\frac{1}{2}, \frac{3}{2}\}$.

2. T Operation

Figure 4(c) indicates that the T operation is applied to a spin- $\frac{1}{2}$ particle, \bullet , and an effective spin- $\frac{1}{2}$ particle, \star . As is clear from Eq. (B1) and the ensuing discussion, the total-spin 1 Hilbert space that we have to consider (after unpacking the effective particle \star) is three-dimensional, and it is spanned by the states

$$(\bullet(\bullet(\bullet\bullet)_b)_c)_{d=1} \quad (\text{D10})$$

with $bc = 0\frac{1}{2}$, $bc = 1\frac{1}{2}$ and $bc = 1\frac{3}{2}$.

An important condition placed on T is that it conserve the quantum number c , which, being the total spin of the qubit with state label b in Fig. 1(b), is initialized to be

$\frac{1}{2}$. We therefore seek the matrix representation of T in what we here call the T -basis,

$$(\bullet(\bullet(\bullet\bullet)_b)_{c=1/2})_{d=1}, \quad b = \{0, 1\}, \quad (\text{D11})$$

with the indicated basis ordering $b = \{0, 1\}$. Labeling these four spins from left to right by 1 through 4 [see also Fig. 11(a)], the T operation can be written as in Eq. (B2),

$$T = U_{34}(2s)V^{-1}U_{12}(t)U_{34}(t)V. \quad (\text{D12})$$

Here $s = 2 - t$, and the pulse sequence for V is given in Fig. 11(d).

We first consider the central two pulses within T , $U_{12}(t)U_{34}(t)$. According to Fig. 11(b), the matrix representation of this operation (up to an overall phase) in the four-spin basis $((\bullet\bullet)_{b'}(\bullet\bullet)_b)_1$ with basis ordering $bb' = \{01, 10, 11\}$ is

$$[U_{12}(t)U_{34}(t)]_{bb'} = e^{-i2\pi t} \text{diag}(e^{i\pi t}, e^{i\pi t}, 1), \quad (\text{D13})$$

Here the subscript in the notation $[U_{12}(t)U_{34}(t)]_{bb'}$ indicates evaluation in the bb' basis.

The V -sequence for the T -gate can, as indicated by the dashed line in Fig. 11(d), be formally divided into two parts,

$$V = U_{23}(\frac{3}{2})U_{12}(\frac{1}{2})U_{34}(\frac{3}{2})U_{23}(\frac{1}{2}) \equiv V_0V_1, \quad (\text{D14})$$

where $V_0 = U_{23}(\frac{3}{2})U_{12}(\frac{1}{2})$ and $V_1 = U_{34}(\frac{3}{2})U_{23}(\frac{1}{2})$. Combining Eqs. (D12) and (D14), we have

$$T = U_{34}(2s)V_1^{-1}V_0^{-1}U_{12}(t)U_{34}(t)V_0V_1. \quad (\text{D15})$$

To find the matrix representation of this T -operation (D15), we now perform a step-by-step evaluation of each of the operations surrounding the central two pulses $U_{12}(t)U_{34}(t)$.

Given that the operation V_0 satisfies the constraint shown in Fig. 11(c), it maps a certain normalized superposition of the $c = \frac{1}{2}$ -states $(\bullet(\bullet(\bullet\bullet)_b)_{c=1/2})_1$ with $b = 0$ and 1 to the state

$$v_1 = ((\bullet\bullet)_{b'=1}(\bullet\bullet)_{b=1})_1. \quad (\text{D16})$$

Due to unitarity, the perpendicular superposition of the same $c = \frac{1}{2}$ -states is mapped into the $bb' = 01, 10$ sector onto the state

$$v_2 = \alpha((\bullet\bullet)_1(\bullet\bullet)_0)_1 + \beta((\bullet\bullet)_0(\bullet\bullet)_1)_1 \quad (\text{D17})$$

with $\alpha = -\frac{2+i}{\sqrt{6}}$ and $\beta = \frac{i}{\sqrt{6}}$ [42]. The action of the similarity transformation carried out by V_0 in Eq. (D12) can thus be viewed as a basis change from the T -basis (D11) to the v -basis $\{v_1, v_2\}$,

$$v_i = \sum_{b=0,1} F_0^{v_i b} (\bullet(\bullet(\bullet\bullet)_b)_{1/2})_1. \quad (\text{D18})$$

The coefficients $F_0^{v_i b}$ are given by

$$F_0^{v_i b} = \langle v_i | V_0 | (\bullet(\bullet(\bullet\bullet)_b)_{1/2})_1 \rangle. \quad (\text{D19})$$

To find the coefficients of F_0 , we note

$$\langle v_1 | U_{23}(\frac{3}{2})U_{12}(\frac{1}{2}) | (\bullet(\bullet(\bullet\bullet)_b)_{b=0})_{1/2} \rangle_1 = -\frac{1}{2}, \quad (\text{D20})$$

$$\langle v_1 | U_{23}(\frac{3}{2})U_{12}(\frac{1}{2}) | (\bullet(\bullet(\bullet\bullet)_b)_{b=1})_{1/2} \rangle_1 = \frac{\sqrt{3}i}{2}. \quad (\text{D21})$$

These overlaps can be computed straightforwardly by evaluating U_{12} in the basis $((\bullet\bullet)_{b'}(\bullet\bullet)_b)_1$ and U_{23} in the basis $(\bullet((\bullet\bullet)_{b''}\bullet)_c)_1$ using Eq. (1) (with an appropriate choice for the overall phase), together with Eqs. (D3) and (D6). Accordingly, the matrix

$$F_0 = \begin{pmatrix} -1/2 & \sqrt{3}i/2 \\ -\sqrt{3}i/2 & 1/2 \end{pmatrix} = \hat{\mathbf{f}}_0 \cdot \boldsymbol{\sigma} \quad (\text{D22})$$

with $\hat{\mathbf{f}}_0 = (0, -\sqrt{3}/2, -1/2)$ maps the T -basis (D11) to the v -basis $\{v_1, v_2\}$. [We note that this choice of v -basis ordering corresponds to $F_0 = F_0^\dagger$.]

Notice that $U_{12}(t)U_{34}(t)$ as given in Eq. (D13) multiplies each state (D16) and (D17) by a certain phase factor; it is thus diagonal in the v -basis,

$$\begin{aligned} [U_{12}(t)U_{34}(t)]_{v_i} &= e^{-i2\pi t} \text{diag}(1, e^{i\pi t}) \\ &= e^{-i3\pi t/2} e^{-i\pi t \hat{\mathbf{z}} \cdot \boldsymbol{\sigma}/2}. \end{aligned} \quad (\text{D23})$$

To examine the effect of the innermost similarity transformation due to V_0 in Eq. (D15), we let

$$T_0 = V_0^{-1}U_{12}(t)U_{34}(t)V_0. \quad (\text{D24})$$

We evaluate this operation T_0 by carrying out the basis change (D18) to the T -basis,

$$\begin{aligned} T_{0,b} &= e^{-i3\pi t/2} F_0 e^{-i\pi t \hat{\mathbf{z}} \cdot \boldsymbol{\sigma}/2} F_0 \\ &= e^{-i3\pi t/2} e^{-i\pi t \hat{\mathbf{n}}_0 \cdot \boldsymbol{\sigma}/2}, \end{aligned} \quad (\text{D25})$$

where

$$\hat{\mathbf{n}}_0 = 2(\hat{\mathbf{f}}_0 \cdot \hat{\mathbf{z}})\hat{\mathbf{f}}_0 - \hat{\mathbf{z}} = (0, \sqrt{3}/2, -1/2). \quad (\text{D26})$$

We note that the T_0 -sequence (D24) for $t = 1$ equals the R sequence shown in Fig. 3(a), which was used in deriving the Fong-Wandzura sequence [33]. According to the matrix representation (7) of R in the basis $(\bullet(\bullet(\bullet\bullet)_b)_{1/2})_d = (\bullet\star)_d$, we have $R = M$ for $d = 1$. In this basis, which corresponds to the T -basis (D11), the matrix M is then

$$M = T_{0,b} \Big|_{t=1} \stackrel{(D25)}{=} e^{-i3\pi/2} e^{-i\pi \hat{\mathbf{n}}_0 \cdot \boldsymbol{\sigma}/2} = \hat{\mathbf{n}}_0 \cdot \boldsymbol{\sigma}. \quad (\text{D27})$$

We now determine the matrix representations of each of the remaining pulses of the T -sequence (D15) in the T -basis (D11). The operation $U_{34}(t)$ can be evaluated directly in this basis using Eq. (2),

$$U_{34,b}(t) = e^{-i\pi t/2} e^{i\pi t \hat{\mathbf{z}} \cdot \boldsymbol{\sigma}/2}. \quad (\text{D28})$$

The action of $U_{23}(t)$ can be found directly in the basis $(\bullet((\bullet\bullet)_{b''}\bullet)_{1/2})_0$ with $b'' = \{0, 1\}$ using Eq. (2),

$$U_{23,b''}(t) = e^{-i\pi t/2} e^{i\pi t \hat{\mathbf{z}} \cdot \boldsymbol{\sigma}/2}. \quad (\text{D29})$$

To find the matrix of this pulse in the T -basis, we carry out the basis change (D1) to find

$$U_{23,b}(t) = F_1 U_{23,b''}(t) F_1. \quad (\text{D30})$$

Having determined every operation of the T -sequence in the T -basis (D11), we from now on work exclusively in this basis and drop the additional subscripts indicating the current basis. To determine the effect of the outer similarity transformation in Eq. (D15) due to $V_1 = U_{34}(\frac{3}{2})U_{23}(\frac{1}{2})$, we first simplify V_1 as follows,

$$\begin{aligned} V_1 &= U_{34}(\frac{3}{2})U_{23}(\frac{1}{2}) \\ &\stackrel{(D28), (D30)}{=} e^{-i(\pi/2)\hat{\mathbf{z}} \cdot \boldsymbol{\sigma}/2} [F_1 e^{i(\pi/2)\hat{\mathbf{z}} \cdot \boldsymbol{\sigma}/2} F_1] \\ &= [e^{-i(\pi/2)\hat{\mathbf{z}} \cdot \boldsymbol{\sigma}/2} F_1 e^{i(\pi/2)\hat{\mathbf{z}} \cdot \boldsymbol{\sigma}/2}] F_1 \\ &\equiv F_4 F_1, \end{aligned} \quad (\text{D31})$$

so that

$$V_1^{-1} T_0 V_1 = F_1 F_4 T_0 F_4 F_1. \quad (\text{D32})$$

Here, the matrix $F_4 = e^{-i(\pi/2)\hat{\mathbf{z}} \cdot \boldsymbol{\sigma}/2} F_1 e^{i(\pi/2)\hat{\mathbf{z}} \cdot \boldsymbol{\sigma}/2}$ is the result of carrying out a similarity transformation on F_1 ,

$$F_4 = \hat{\mathbf{f}}_4 \cdot \boldsymbol{\sigma} = \begin{pmatrix} -1/2 & -i\sqrt{3}/2 \\ i\sqrt{3}/2 & 1/2 \end{pmatrix} = F_4^\dagger, \quad (\text{D33})$$

where $\hat{\mathbf{f}}_4 = (0, \sqrt{3}/2, -1/2)$ is the result of rotating $\hat{\mathbf{f}}_1 = (\sqrt{3}/2, 0, -1/2)$ through an angle of $-\pi/2$ about the z axis. Note that $\hat{\mathbf{f}}_4 = \hat{\mathbf{n}}_0$, because of which the F_4 matrix in Eq. (D32) commutes with $T_0 \sim e^{-i\pi t \hat{\mathbf{n}}_0 \cdot \boldsymbol{\sigma}/2}$ and thus has no effect, allowing us to simplify

$$\begin{aligned} V_1^{-1} T_0 V_1 &= e^{-i3\pi t/2} [F_1 e^{-i\pi t \hat{\mathbf{n}}_0 \cdot \boldsymbol{\sigma}/2} F_1] \\ &= e^{-i3\pi t/2} e^{-i\pi t \hat{\mathbf{n}}_1 \cdot \boldsymbol{\sigma}/2} \end{aligned} \quad (\text{D34})$$

with $\hat{\mathbf{n}}_1 = 2(\hat{\mathbf{n}}_0 \cdot \hat{\mathbf{f}}_1)\hat{\mathbf{f}}_1 - \hat{\mathbf{n}}_0 = (\sqrt{3}/4, -\sqrt{3}/2, 1/4)$. The matrix representation of the operation due to the last pulse, $U_{34}(2s)$, is given in Eq. (D28), so that

$$\begin{aligned} T &= U_{34}(2s) V_1^{-1} T_0 V_1 \\ &= [e^{-i2\pi s/2} e^{i2\pi s \hat{\mathbf{z}} \cdot \boldsymbol{\sigma}/2}] [e^{-i3\pi t/2} e^{-i\pi t \hat{\mathbf{n}}_1 \cdot \boldsymbol{\sigma}/2}] \\ &= e^{-i\pi t/2} e^{i\pi(2-t)\hat{\mathbf{z}} \cdot \boldsymbol{\sigma}} e^{-i\pi t \hat{\mathbf{n}}_1 \cdot \boldsymbol{\sigma}/2} \end{aligned} \quad (\text{D35})$$

where we used $s = 2 - t$.

Finally, associating this result (D35) given in the T -basis, that is $(\bullet(\bullet(\bullet\bullet)_b)_{1/2})_{d=1} = (\bullet\star)_{d=1}$, with the matrix \mathbb{M} in Eq. (8), we conclude

$$\begin{aligned} \mathbb{M} &= e^{-i\pi t/2} e^{i\pi(2-t)\hat{\mathbf{z}} \cdot \boldsymbol{\sigma}} e^{-i\pi t \hat{\mathbf{n}}_1 \cdot \boldsymbol{\sigma}/2} \\ &\equiv e^{i\pi t/2} e^{i\phi(t)\hat{\mathbf{n}}(t) \cdot \boldsymbol{\sigma}/2} \end{aligned} \quad (\text{D36})$$

with the effective rotation angle $\phi(t) = 2 \arccos((5 \cos(\pi t/2) + 3 \cos(3\pi t/2))/8)$ and a unit vector $\hat{\mathbf{n}}(t)$. Since $\phi(0) = 0$ and $\phi(t_1 \equiv 4 \arctan(\sqrt{2 - \sqrt{3}})) = 2\pi$ the pulse sequence constructed in Sec. III can thus be used to carry out arbitrary controlled rotation gates using values of $t \in [0, t_1]$.

3. Pseudospin Transformation

In Appendix C we use a transformation from one pseudospin space, which is spanned by the states

$$\uparrow_{1/2} = (\blacktriangle(\bullet\blacktriangle)_{c=1/2})_{1/2}, \quad \downarrow_{1/2} = (\blacktriangle(\bullet\blacktriangle)_{c=3/2})_{1/2}, \quad (\text{D37})$$

to another pseudospin space spanned by

$$\uparrow'_{1/2} = (\blacktriangle(\blacktriangle\bullet)_{c=1/2})_{1/2}, \quad \downarrow'_{1/2} = (\blacktriangle(\blacktriangle\bullet)_{c=3/2})_{1/2}. \quad (\text{D38})$$

This change of bases is carried out by a generalized SWAP, denoted U in this section, which exchanges the rightmost effective spin-1, \blacktriangle , with the spin- $\frac{1}{2}$, \bullet . Taking into account that the total spin of these two particles, c , is conserved, and ignoring the leftmost \blacktriangle in the above pseudospin states (which remains unchanged by this transformation), we write

$$U |(\bullet\blacktriangle)_c \rangle = F_c |(\blacktriangle\bullet)_c \rangle. \quad (\text{D39})$$

The basis change from $(\bullet\blacktriangle)_c$ to $(\blacktriangle\bullet)_c$ with $c = \{\frac{1}{2}, \frac{3}{2}\}$ is thus characterized by a diagonal matrix $F = \text{diag}(F_{c=1/2}, F_{c=3/2})$.

Figure 13 shows the basic information required to understand the basis change (D39). As shown in Fig. 13(a), we replace the spin-1 particle by two spin- $\frac{1}{2}$ particles with total spin 1,

$$(\bullet\blacktriangle)_c \rightarrow (\bullet(\bullet\bullet)_{a=1})_c. \quad (\text{D40})$$

The full Hilbert space of three spin- $\frac{1}{2}$ particles is spanned by the states $(\bullet(\bullet\bullet)_a)_c$ with $ac = 0\frac{1}{2}$, $ac = 1\frac{1}{2}$ and $ac = 1\frac{3}{2}$. Again referring to Fig. 13(a), this basis change is then carried out by

$$U = U_{23}(1)U_{12}(1), \quad (\text{D41})$$

where we labeled the spins 1 through 3 from left to right (or top to bottom in Fig. 13). The action of these SWAPs can be computed straightforwardly using simple spin wave functions; however, in the spirit of this work, we commit, as we have throughout, to using only total spin quantum numbers and recoupling coefficients, adopting the Condon-Shortley phase convention.

The transformation (D39) now reads

$$U |(\bullet(\bullet\bullet)_{a=1})_c \rangle = F_c |((\bullet\bullet)_{a'=1}\bullet)_c \rangle, \quad (\text{D42})$$

where the coefficients are determined by

$$F_c = \langle ((\bullet\bullet)_1\bullet)_c | U |(\bullet(\bullet\bullet)_1)_c \rangle. \quad (\text{D43})$$

Note that the states on either side of this equation are given in different bases. In the case of total spin $c = \frac{3}{2}$ the transformation between these bases is trivial,

$$\langle ((\bullet\bullet)_1\bullet)_{3/2} | = \langle ((\bullet(\bullet\bullet)_1)_{3/2} |, \quad (\text{D44})$$

so that here a SWAP acting on the two leftmost spins has the same effect as a SWAP acting on the two rightmost spins. From Eq. (1) for the case of $a = 1$ we find

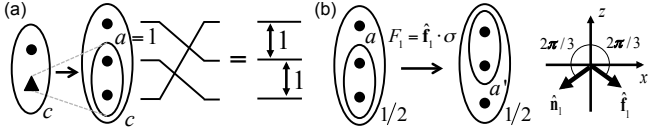


FIG. 13. Generalized SWAP operation (D39) consisting of, (a), two regular SWAPS followed by, (b), basis change carried out by F_1 . In (a), the effective spin-1, \blacktriangle , is replaced with two spin- $\frac{1}{2}$ particles, \bullet , with total spin $a = 1$.

$U_{12}^{c=3/2}(1) = U_{23}^{c=3/2}(1) = e^{-i\pi} = -1$. Using Eq. (D41) we obtain for $c = \frac{3}{2}$ that $U^{c=3/2} = (-1)^2 = 1$, so that

$$F_{c=3/2} = \langle (\bullet(\bullet\bullet)_1)_{3/2} | U^{c=3/2} | (\bullet(\bullet\bullet)_1)_{3/2} \rangle = 1. \quad (\text{D45})$$

For the two-dimensional $c = \frac{1}{2}$ sector using the matrix F_1 given in Eq. (D3), the $c = 1/2$ equivalent of Eq. (D44) is

$$\langle ((\bullet\bullet)_1\bullet)_{1/2} | = \sum_{a=0,1} F_{1,1a} \langle (\bullet(\bullet\bullet)_a)_{1/2} |, \quad (\text{D46})$$

where we have used $F_1^\dagger = F_1$.

Combining Eqs. (D43) for $c = \frac{1}{2}$ and (D46) we obtain

$$F_{c=1/2} = \sum_{a=0,1} F_{1,1a} \langle (\bullet(\bullet\bullet)_a)_{1/2} | U^{c=1/2} | (\bullet(\bullet\bullet)_1)_{1/2} \rangle. \quad (\text{D47})$$

To find this matrix element, let us first determine the matrix representations of the two SWAPS making up U

for total spin $c = \frac{1}{2}$. The matrix of $U_{23}(1)$ in the basis $(\bullet(\bullet\bullet)_a)_{1/2}$ with state ordering $a = \{0, 1\}$ is given by Eq. (2) for $t = 1$, $U_{23}^{c=1/2}(1) = e^{-i\pi/2} e^{i\pi\hat{z}\cdot\sigma/2}$. Similarly, in the alternate basis $((\bullet\bullet)_a\bullet)_{1/2}$ with $a' = \{0, 1\}$ the matrix of $U_{12}(1)$ is also given by Eq. (2) for $t = 1$. Changing from this a' basis to the a basis given above, we have $U_{12}^{c=1/2}(1) = F_1 e^{-i\pi/2} e^{i\pi\hat{z}\cdot\sigma/2} F_1$.

In the basis $a = \{0, 1\}$, the operator $F_1 U^{c=1/2}$ is then

$$\begin{aligned} F_1 U^{c=1/2} &= F_1 e^{-i\pi/2} e^{i\pi\hat{z}\cdot\sigma/2} (F_1 e^{-i\pi/2} e^{i\pi\hat{z}\cdot\sigma/2} F_1) \\ &\equiv F_1 F'_1 F_1, \end{aligned} \quad (\text{D48})$$

where $F'_1 = (e^{-i\pi/2} e^{i\pi\hat{z}\cdot\sigma/2}) F_1 (e^{-i\pi/2} e^{i\pi\hat{z}\cdot\sigma/2}) = \hat{f}'_1 \cdot \sigma$. The vector $\hat{f}'_1 = (-\sqrt{3}/2, 0, -1/2)$ is the result of rotating \hat{f}_1 through π about the z axis. With reference to Fig. 13(b), we evaluate $F_1 F'_1 F_1$ noting that rotating the vector \hat{f}'_1 through π about \hat{f}_1 results in the vector \hat{z} , implying that $F_1 U^{c=1/2} = e^{-i\pi/2} e^{i\pi\sigma_z/2} = \text{diag}(1, -1)$ in the usual basis ordering $a = \{0, 1\}$. Equation (D47) thus yields

$$F_{c=1/2} = \sum_{a=0,1} F_{1,1a} \langle (\bullet(\bullet\bullet)_a)_{1/2} | U^{c=1/2} | (\bullet(\bullet\bullet)_1)_{1/2} \rangle = -1. \quad (\text{D49})$$

We conclude that the basis change (D39) is carried out by the matrix

$$F = \text{diag}(F_{c=1/2}, F_{c=3/2}) = \text{diag}(-1, 1). \quad (\text{D50})$$

This operation can be interpreted as a z -axis rotation through π when performing the pseudospin transformation from Eq. (D37) to (D38) via the generalized SWAP.

[1] D. Loss and D. P. DiVincenzo, Phys. Rev. A **57**, 120 (1998).
[2] J. Levy, Phys. Rev. Lett. **89**, 147902 (2002).
[3] D. Bacon, J. Kempe, D. A. Lidar, and K. B. Whaley, Phys. Rev. Lett. **85**, 1758 (2000).
[4] J. Kempe, D. Bacon, D. A. Lidar, and K. B. Whaley, Phys. Rev. A **63**, 042307 (2001).
[5] M. Russ and G. Burkard, Journal of Physics: Condensed Matter **29**, 393001 (2017).
[6] D. P. DiVincenzo, D. Bacon, J. Kempe, G. Burkard, and K. B. Whaley, Nature **408**, 339 (2000).
[7] Y. S. Weinstein and C. S. Hellberg, Phys. Rev. A **72**, 022319 (2005).
[8] Z. Shi, C. B. Simmons, J. R. Prance, J. K. Gamble, T. S. Koh, Y.-P. Shim, X. Hu, D. E. Savage, M. G. Lagally, M. A. Eriksson, M. Friesen, and S. N. Coppersmith, Phys. Rev. Lett. **108**, 140503 (2012).
[9] T. S. Koh, J. K. Gamble, M. Friesen, M. A. Eriksson, and S. N. Coppersmith, Phys. Rev. Lett. **109**, 250503 (2012).
[10] J. M. Taylor, V. Srinivasa, and J. Medford, Phys. Rev. Lett. **111**, 050502 (2013).
[11] A. C. Doherty and M. P. Wardrop, Phys. Rev. Lett. **111**, 050503 (2013).
[12] M. De Michielis, E. Ferraro, M. Fanciulli, and E. Prati, Journal of Physics A: Mathematical and Theoretical **48**, 065304 (2015).
[13] Y.-P. Shim and C. Tahan, Phys. Rev. B **93**, 121410 (2016).
[14] M. P. Wardrop and A. C. Doherty, Physical Review B **93**, 075436 (2016).
[15] B.-C. Wang, G. Cao, H.-O. Li, M. Xiao, G.-C. Guo, X. Hu, H.-W. Jiang, and G.-P. Guo, Physical Review Applied **8**, 064035 (2017).
[16] T. D. Ladd and C. Jones, arXiv preprint arXiv:1712.05849 (2017).
[17] Y. Kawano, K. Kimura, H. Sekigawa, M. Noro, K. Shirayanagi, M. Kitagawa, and M. Ozawa, Quantum Information Processing **4**, 65 (2005).
[18] J. Petta, A. Johnson, J. Taylor, E. Laird, A. Yacoby, M. Lukin, C. Marcus, M. Hanson, and A. Gossard, Science **309**, 2180 (2005).
[19] E. A. Laird, J. M. Taylor, D. P. DiVincenzo, C. M. Marcus, M. P. Hanson, and A. C. Gossard, Phys. Rev. B **82**, 075403 (2010).
[20] L. Gaudreau, G. Granger, A. Kam, G. Aers, S. Stukenikin, P. Zawadzki, M. Pioro-Ladriere, Z. Wasilewski, and A. Sachrajda, Nature Physics **8**, 54 (2012).

[21] J. Medford, J. Beil, J. Taylor, S. Bartlett, A. Doherty, E. Rashba, D. DiVincenzo, H. Lu, A. Gossard, and C. Marcus, *Nature Nanotechnology* **8** (2013).

[22] J. Medford, J. Beil, J. M. Taylor, E. I. Rashba, H. Lu, A. C. Gossard, and C. M. Marcus, *Phys. Rev. Lett.* **111**, 050501 (2013).

[23] D. Kim, Z. Shi, C. Simmons, D. Ward, J. Prance, T. S. Koh, J. K. Gamble, D. Savage, M. Lagally, M. Friesen, *et al.*, *Nature* **511**, 70 (2014).

[24] K. Eng, T. D. Ladd, A. Smith, M. G. Borselli, A. A. Kiselev, B. H. Fong, K. S. Holabird, T. M. Hazard, B. Huang, P. W. Deelman, I. Milosavljevic, A. E. Schmitz, R. S. Ross, M. F. Gyure, and A. T. Hunter, *Science Advances* **1** (2015), 10.1126/sciadv.1500214.

[25] M. D. Reed, B. M. Maune, R. W. Andrews, M. G. Borselli, K. Eng, M. P. Jura, A. A. Kiselev, T. D. Ladd, S. T. Merkel, I. Milosavljevic, E. J. Pritchett, M. T. Rakher, R. S. Ross, A. E. Schmitz, A. Smith, J. A. Wright, M. F. Gyure, and A. T. Hunter, *Phys. Rev. Lett.* **116**, 110402 (2016).

[26] G. Cao, H.-O. Li, G.-D. Yu, B.-C. Wang, B.-B. Chen, X.-X. Song, M. Xiao, G.-C. Guo, H.-W. Jiang, X. Hu, *et al.*, *Physical review letters* **116**, 086801 (2016).

[27] B. Thorgrimsson, D. Kim, Y.-C. Yang, L. Smith, C. Simmons, D. R. Ward, R. H. Foote, J. Corrigan, D. Savage, M. Lagally, *et al.*, *npj Quantum Information* **3**, 32 (2017).

[28] R. W. Andrews, C. Jones, M. D. Reed, A. M. Jones, S. D. Ha, M. P. Jura, J. Kerckhoff, M. Levendorf, S. Meenehan, S. T. Merkel, *et al.*, *Nature nanotechnology* **14**, 747 (2019).

[29] M. Hsieh, J. Kempe, S. Myrgren, and K. B. Whaley, *Quantum Information Processing* **2**, 289 (2003).

[30] B. H. Fong and S. M. Wandzura, *Quantum Information & Computation* **11**, 1003 (2011).

[31] F. Setiawan, H.-Y. Hui, J. Kestner, and X. Wang, *Bulletin of the American Physical Society* **59** (2014).

[32] The definition of an optimal pulse sequence is ambiguous. Here, by optimal we mean requiring the least number of pulses for spins oriented along a linear array, assuming the exchange coupling can only be turned on between nearest neighbors.

[33] D. Zeuch and N. E. Bonesteel, *Phys. Rev. A* **93**, 010303 (2016).

[34] D. Zeuch, R. Cipri, and N. E. Bonesteel, *Phys. Rev. B* **90**, 045306 (2014).

[35] M. A. Nielsen and I. L. Chuang, *Quantum computation and quantum information* (Cambridge university press, 2010).

[36] J. R. van Meter and E. Knill, *Physical Review A* **99**, 042331 (2019).

[37] In Appendix D 2, the vector $\hat{\mathbf{n}}_0$ is explicitly calculated for the Condon-Shortley phase convention, see Eqs. (D26) and (D27).

[38] The vector $\hat{\mathbf{n}}_2$, and all vectors in the various pseudospin spaces discussed in this paper, can be rotated about the z axis by multiplying the total-spin basis states by different phase factors. To fix this gauge degree of freedom we adopt the standard Condon-Shortley phase convention, as discussed in Appendix D 1.

[39] It has come to our attention that 24-pulse sequences (not counting single-qubit operations) which carry out arbitrary CPHASE gates for spins oriented on a linear array can be found through numerical search. Bryan Fong (private communication).

[40] We note that the constraint for the T operation posed by Eq. (8), because of which we use the non-optimal V sequence shown in Fig. 11(d), can be relaxed by letting $T = (\mathbb{M}_1, \mathbb{M}_2)$, given in the same basis as Eq. (8). If $\mathbb{M}_1 \mathbb{M}_2^{-1} \neq e^{i\delta} \mathbb{1}$ for some phase δ , the corresponding sequence shown in Fig. 4(c) enacts a leakage-free, entangling two-qubit gate. The shortest sequence for T of the form (B2) is then $T = V_0^{-1} U_{12}(t) U_{34}(t) V_0$. However, one can show that either choice of T yields the same two-qubit gate sequence (up to single-qubit rotations).

[41] A. Messiah, Appendix C (Section IV) (North-Holland Publishing Company, Amsterdam, 1969) (1962).

[42] The values for α and β , given here for completeness, are not relevant for our discussion, since the operation $U_{12}(t) U_{34}(t)$ acts as the identity in the $bb'd = 011, 101$ sector, see Eq. (D13).